LUND UNIVERSITY
Faculty of Science

Background Studies of the High-Intensity Baryon Extraction and Measurement (HIBEAM) Experiment at the European Spallation Source

Author: Blahoslav Rataj

Thesis submitted for the degree of Master of Science
Supervised by David Silvermyr and Valentina Santoro
Project duration: 4 months
Department: Department of Physics
Division: Particle Physics
Date: June 2021

Abstract

The High-Intensity Baryon Extraction and Measurement experiment (HIBEAM) is proposed as one of the experimental stations at the European Spallation Source (ESS). This experiment will mainly focus on the neutron into sterile neutron oscillations which violate the baryon number (B) by one unit. The sterile neutrons are hypothetical dark matter candidates. The neutrons suitable for the experiment have energy lower than approximately 1 eV and are transported from the moderator of the ESS into HIBEAM by the ANNI (a pulsed cold neutron beam facility) beamline. The goal of this thesis was to estimate the neutron background and radiation dose rate for the ANNI beamline using simulations performed with the Particle and Heavy Ion Transport code System (PHITS). This study is supported by the need to reach a high sensitivity of the neutron into sterile neutron oscillation experiments. The sensitivity of such experiments strongly depends on the magnitude of the background. The detailed model of the ANNI beamline was implemented and integrated into the ESS target model. The neutron spectrum at 22 m from the center of the ESS target monolith was calculated with a two-step calculation process in order to transport the neutrons through such a long guiding system that extends from 2 m relative to the ESS target monolith. It was found that the flux of high-energy (fast) neutrons that are the source of background significantly reduced between the ANNI opening and the entrance to the HIBEAM experimental area at 22 m relative to the target monolith. Nevertheless, the design of the neutron guide system of ANNI could be improved because a significant fraction of the fast neutrons were not stopped inside the bunker wall. Consequently, the fast neutrons contributed to observed large dose levels outside the bunker wall edge located at a distance of 15 m from the target monolith. Different thicknesses of the shielding material outside the bunker wall edge were tested, but even 70 cm thick block of high-density concrete was not capable of stopping fast neutron below the acceptable value of the effective dose of 1.5 μSv/h. This project can be used as a ground for the optimization of the geometric model of the ANNI beamline. The results of this project can also support the future ANNI beamline proposal.

Acknowledgement

I would like to express my special thanks to my co-supervisor Dr. Valentina Santoro as well as my supervisor Dr. David Silvermyr, who gave me the opportunity to work on this project. Their regular feedback on the thesis structure, understanding of the theory and data analysis was a great support for me.

Contents

1 List of Abbreviations

ANNI	A pulsed cold neutron beam facility
CKM	Cabibbo—Kobayashi—Maskawa
CMB	cosmic microwave background
CP	charge parity
CPU	central processing unit
ESS	European Spallation Source
FOC	frame overlap chopper
GUT	grand unified theory
GZK	Greisen—Zatsepin—Kuzmin
HIBEAM	High-Intensity Baryon Extraction and Measurement
LHC	Large Hadron Collider
McStas	Monte carlo Simulation of triple axis spectrometers
NNBAR	neutron-antineutron transformation
PDC	pulse-defining chopper
PHITS	Particle and Heavy Ion Transport code System
SM	Standard Model
UCN	ultracold neutron
VITESS	Virtual Instrumentation Tool for the ESS

2 Introduction

The European Spallation Source (ESS) is a research facility being constructed in the fields on the outskirts of Lund, Sweden. The project is financed and lead by thirteen European countries. ESS will be the world's most powerful neutron source after its completion. There will be twenty-two experimental stations in total. The focus of this thesis is the High-Intensity Baryon Extraction and Measurement (HIBEAM) experiment, which makes use of neutrons coming from the ANNI (a pulsed cold neutron beam facility) beamline [1]: a proposed instrument dedicated to particle and fundamental physics [2].

The experimental focus of HIBEAM is the searches for the neutron to sterile neutron conversions. These processes violate the baryon number (B) by one unit. The HIBEAM experiment represents the first phase of the two-stage programme which second step will be the neutron to antineutron oscillations experiment: neutron-antineutron transformation (NNBAR). The NNBAR experiment will be able to look for the neutron to antineutron ($n \to \bar{n}$) oscillations with an increase in experimental sensitivity by a factor of 10^3 in comparison to the previous experiment performed at ILL [3]. This process violates B by two units.

The sterile sector of particles could represent a possible dark sector [1]. Both aforementioned B violating processes could contribute to various cosmological phenomena. The possible existence of the dark sector is coupled to the problem of dark matter, the dominant and hitherto poorly understood contribution of the matter budget of the Universe. Two main experimental approaches can be used to search for sterile neutrons: measurements of neutrons trapped in an ultra-cold neutron (UCN) bottle and measurements with the beam neutrons. While there have been several measurements with UCN, there is currently no measurement with the beam neutrons.

The goal of HIBEAM is to search for the neutron to sterile neutron transitions with a beam of neutrons for the first time. In addition to the direct transition of $n \to n'$, experiments done with the beam neutrons can also look for different modes, like regeneration of neutrons following a beam stop, and also $n \to \bar{n}$ transition via a sterile neutron state (see section 4.4). These two processes cannot be searched using UCN. It is important to note that the sensitivity of these experiments that will be performed at HIBEAM is strongly coupled to the possibility of achieving low background rates.

The purpose of this thesis is to study the background of the ANNI beamline using a Monte-Carlo radiation transport code called Particle and Heavy Ion Transport code System (PHITS) [4]. A detailed model of the beamline must be implemented, including the simulation of a neutron production at ESS and their subsequent propagation through ANNI. The spectrum is measured to estimate a background made of fast neutrons (i.e. neutrons with energy > 1 eV) at the end of

the ANNI beamline at the location of the HIBEAM experiment. Simultaneously, a dose map is recorded to test shielding effectiveness to stop fast neutrons.

3 Scientific Motivation

3.1 Standard model

The Standard Model (SM) is a theory that characterizes particles and their interactions using a function called Lagrangian. There are three types of particles: matter particles, gauge and scalar bosons. Overview of the constituents of the SM [5] is shown in Figure 1. First, the elementary matter particles correspond to fermions with a half-integer spin called quarks and leptons. Both quarks and leptons can be further classified by six different flavours. Second, the gauge bosons have an integer spin and can mediate interactions between the quarks and leptons. The type of interaction between the quarks and leptons determines which gauge boson is exchanged. The massless photons are interchanged in the case of the electromagnetic interaction, while the massive W and Z bosons are interchanged in the case of the weak interaction. Moreover, the massless gluons are interchanged in the case of the strong interaction. Finally, the scalar, spin-zero Higgs boson is responsible for the mechanism in which the matter particles and massive gauge bosons obtain mass. The interesting property of the SM is that W, Z and Higgs bosons and gluons can also self-interact. The SM is considered to be a gauge theory in the sense that invariance present in the SM interactions gives rise to the exchange of gauge bosons [6].

Apart from the electric charge of the electromagnetic force, each quark possesses a colour charge of the strong force. The nature of the strong force gives rise to the confinement of quarks into a colourless hadron. The hadron made of a quark-antiquark pair is called a meson, while the hadron made of three quarks, or antiquarks is called baryon and antibaryon, respectively [7].

3.2 Models of Baryogenesis

3.2.1 Matter Dominant Universe

The Universe contains significantly more matter than antimatter. Such a statement is possible, for example, based on observations of the primary cosmic rays [8]. The primary cosmic rays can be detected using a satellite just before they reach the Earth's atmosphere. They are mainly composed of protons and alpha particles. Alpha particles contain two protons and neutrons [9]. The possible sources of cosmic rays are not yet fully understood. This especially applies to the most energetic part of the spectrum of the primary cosmic rays [10]. There is a clear

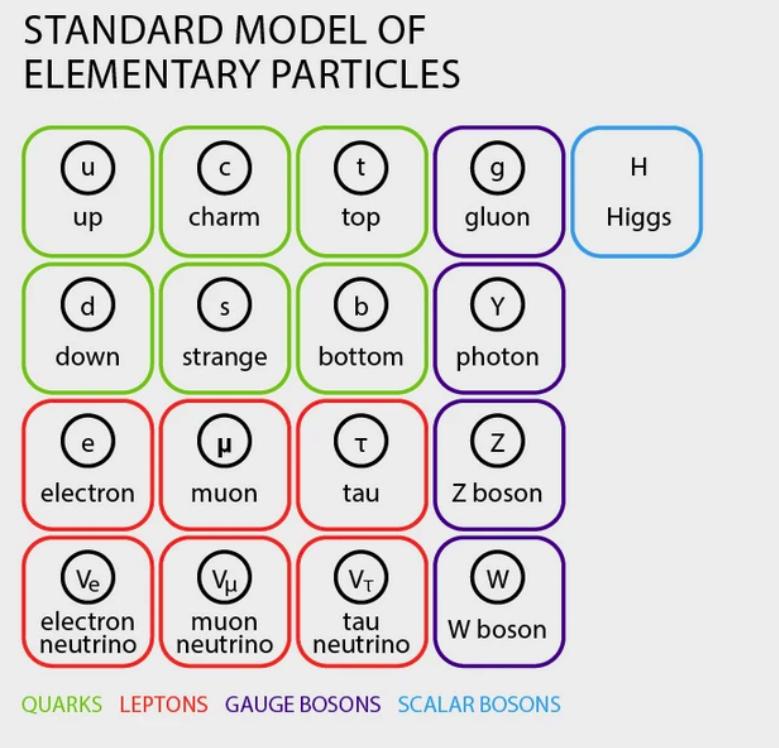

Figure 1: Overview over the particles in the SM. Adapted from ref. 5.

dominance of matter based on the measured ratio of antiprotons to protons in the primary cosmic rays. It turns out that this ratio varies from 10^{-5} to 10^{-4} in the range between 1 to 100 GeV based on measurements of Adriani et al. [11]. Moreover, it is expected that most of the detected antiprotons were produced in the interactions of primary cosmic rays with the interstellar material. Therefore, many detected antiprotons were not produced at the sources of cosmic rays and are treated as secondary particles. The remaining antiprotons are expected to be produced in processes that involve dark matter [12]. The question is whether this observation of the dominance of matter over antimatter can be generalised on the whole Universe. It may be the case that the detected cosmic rays originate from the matter dominant region of the Universe, which can be accompanied by the antimatter dominant region of the Universe. Nevertheless, this hypothesis would require observing gamma rays from the annihilation of matter with antimatter originating from the boundaries of matter and antimatter dominant regions. These gamma rays were not observed [8].

Two independent estimates of the asymmetry parameter show that there already was a slightly higher amount of matter than antimatter in the early times

of the Universe. The asymmetry parameter is defined according to Equation 1:

$$\eta = \frac{n_B - n_{\bar{B}}}{n_B + n_{\bar{B}}} \approx \frac{n_B - n_{\bar{B}}}{s} \tag{1}$$

where n_B is the number of baryons and $n_{\bar{B}}$ is the number of antibaryons. The difference between n_B and $n_{\bar{B}}$ is divided by entropy density s to make Equation 1 invariant under the expansion of the Universe [8]. The first way to estimate the asymmetry parameter is based on the abundances of elements synthesised in the time of the Big Bang nucleosynthesis. The Big Bang nucleosynthesis was a process in which some of the lightest elements, such as D, ^{4}He or ^{7}Li, were produced by a fusion. The process began when the Universe cooled to the temperature of about 10^{10} K. Conditions at this temperature allowed the existence of stable nuclei, and fusion of protons and neutrons was still possible [13]. The value of η was estimated to be approximately 10^{-10} as reported by Fields and Sarkar (Particle Data Group) [14]. The second way to estimate the asymmetry parameter is based on the temperature anisotropy in the cosmic microwave background (CMB). More specifically, the relative height of peaks found on the plot of CMB Temperature vs multipole moment gives η [15]. CMB, sometimes called "a relic radiation", is radiation with the origin in the time when the Universe cooled to about 3000 K. This temperature allowed to form bounded state of nuclei and electrons which significantly minimised the number of times the CMB photons are scattered. This lead to the state that is sometimes called a transparent Universe. CMB gives useful information about the early times of the Universe. The great advantage is that it can be detected on the Earth [16]. η based on the CMB analysis was again estimated to be of the order of 10^{-10} according to Fields and Sarkar [14]. The difference between the number of matter and antimatter particles was therefore tiny in the early times of the Universe. However, even a small excess of matter over antimatter resulted in matter dominant Universe when conditions allowed the antimatter particles to annihilate with matter particles [17]. Sakharov conditions [18] had to be satisfied to initiate baryogenesis. Baryogenesis was a process that led to the creation of a small baryon asymmetry in the early times of the Universe. This asymmetry can be quantified by η as discussed above. Sakharov conditions are the B-violation, charge (C) and charge-parity (CP) symmetry violation and deviation from the thermal equilibrium. All the conditions can be satisfied in different models of baryogenesis which involve novel types of particle interactions.

Sakharov conditions can be satisfied by different processes. First, the exact processes and conditions in which the B can be violated are investigated. One of the predicted processes where B is violated is oscillations of a neutron into sterile/anti neutron [19]. Second, the CP violation is proven to be present in some of the particle interactions, for example, in the decay of D meson [20]. In addition,

the CP violation is predicted by the SM [6] by having a complex phase in the Cabibbo—Kobayashi—Maskawa (CKM) matrix. The CKM matrix leads to mixing between different quark flavours, and predicts the strength of such interactions. Finally, the thermal equilibrium could be broken in the early times, for example, during the first-order electroweak phase transition [21].

3.2.2 Grand Unification Theory and Electroweak Baryogenesis

There are several possible moments during the early development of the Universe when baryogenesis could take place. Namely, the most discussed is the time just after the grand unification epoch and the time during the electroweak epoch when some theories indicate that Sahkarov conditions were satisfied. It is simultaneously expected that the amount of matter and antimatter was equal in the first instants of the Universe. The first moment is related to the model of grand unified theory (GUT) baryogenesis, and the second is related to the model of electroweak baryogenesis. The GUT baryogenesis is the oldest model of baryogenesis [22]. The GUT predicts unification of fundamental the SM forces at the scale of approximately 10^{16} GeV. More specifically, there exists, in the simplest case, the SU(5) group which is spontaneously broken into $SU(3)_C \otimes SU(2)_L \otimes U(1)_Y$, i. e. groups representing the SM internal symmetries (the SM interactions), below the GUT scale [23]. Quarks and leptons are arranged into an object with 5 x 1 components (quintet) and an object with 5 x 5 components in this theory. Then, there are 24 generators of SU(5) arranged in an object again with 5 x 5 components giving rise to the X and Y bosons, which are not present in the SM interactions [6]. Computation of the interaction Lagrangian reveals that X and Y bosons can mediate B violating interactions between fermions [22]. For example, the X boson can couple to uu, or $e^+ \bar{d}$ [6]. Therefore, B can be violated in vertices involving the X boson [23]. However, the GUT baryogenesis can be rejected, for example, based on the assumption that the Universe reached a temperature of about 10^{13} GeV after the inflation. This temperature is below the GUT energy scale [22].

Electroweak baryogenesis fits better into a modern cosmology. The baryogenesis would be initiated when the temperature of the Universe dropped to approximately 100 GeV. The electroweak symmetry ($SU(2)_L \otimes U(1)_Y$) was spontaneously broken into $U(1)_{EM}$ at this temperature, and nature picked one of the vacuum states giving rise to Higgs field. All the Sakharov conditions, including B violation, could be satisfied during this process of spontaneous breaking of the symmetry. There could be "bubbles" formed with the broken phase where the sphaleron process could take place and would be out of equilibrium that would lead to net asymmetry between density of baryons and antibaryons [24]. The sphaleron process relates to transitions (tunnelling) between different vacuum states. B + L, where L is the lepton number, is violated during the tunnelling interactions [22].

One of the problems with the model of electroweak baryogenesis is that it expects that Higgs mass is below approximately 70 GeV, such that the first-order transition could take place [24]. However, the currently accepted value of the Higgs mass determined experimentally is approximately 125 GeV [25].

The GUT scale is much larger than the energies present in the interactions at the Large Hadron Collider (LHC). However, GUTs predict different limits on proton decays. These limits can be tested experimentally. Most of GUTs can be then rejected since their prediction of the proton lifetime seems to be incorrect based on the experiments. No proton decays were actually observed [26]. The electroweak energy scales are easier to reach in the high-energy experiments, including the LHC, so the electroweak phase transition and baryogenesis can be potentially verified experimentally [27].

3.2.3 Post-Sphaleron Baryogenesis

In addition, there is a model of post-sphaleron baryogenesis, which would involve conversions of neutrons into antineutrons. This model predicts the existence of a scalar boson S_r which can interact with three colour-sextet diquark scalar fields that can decay into six quarks or antiquarks. Then, there would exist a high dimensional operator O that can couple to S_r resulting in a B violating process. Consequently, the neutron-antineutron oscillations which violate B by two units would become possible as this process would involve the identical diquark scalar field couplings as the decay of S_r [28]. The whole process involving the exchange of S_r could take place when the temperature of the Universe was in the range between 0.1 and 100 GeV, i. e. after the expected time of electroweak baryogenesis. S_r and its decay mechanism arises from the Pati–Salam symmetry group $SU(2)_L \otimes\ SU(2)_R \otimes\ SU(4)_C$. The Pati–Salam symmetry group can be spontaneously broken from the SO(10) GUT [29]. The energy scale of the diquark scalar fields is approximately expected to be in the order of TeV such that these fields can potentially be produced and studied, for example, at the LHC [30]. A different possibility is to search directly for the neutron-antineutron oscillations in the experiments with a large number of low energy neutrons as it is mainly planned for the NNBAR experiment at ESS [1].

3.3 Mirror Matter

3.3.1 Definition

The weak interaction is mediated only between left-handed particles or right-handed antiparticles with respect to their chirality, such that the SM is not symmetric under the parity transformation operator. The parity represents a discrete

symmetry in the SM with x $\rightarrow$ -x [31]. A clear violation of parity in the SM gave rise to theories of a possible existence of a mirror sector of particles. The reason is that the weak force is predicted to be mediated rather between the right-handed particles and left-handed antiparticles in the mirror sector. Therefore, the transformations of particles in mirror particles would conserve the parity. The hypothesised mirror sector of particles consists of the identical particles that are known from the ordinary sector of particles. More specifically, each left-handed fermion in the ordinary sector is hypothesised to have a right-handed partner in the mirror sector. Moreover, the interactions between the mirror particles should stem from the same local gauge symmetries leading to the identical mechanism of interactions between mirror particles by exchanging corresponding mirror bosons. This can be easily represented by adopting the ordinary matter gauge symmetry G = $U(1)_Y \otimes SU(2)_L \otimes SU(3)_C$ to write the mirror matter gauge symmetry $G^{'} = U(1)_Y^{'} \otimes SU(2)_R^{'} \otimes SU(3)_C^{'}$ [32] such that the ordinary matter particles are singlets with respect to $G^{'}$. This indicates that the possible interaction mechanisms between the mirror particles with the ordinary matter particles are limited. Therefore, the mirror particles are invisible in experiments sensitive to the electroweak and strong interactions between ordinary matter particles only. Consequently, the mirror sector of particles is considered to be one of the dark matter candidates [19]. The interactions between the mirror and ordinary matter particles are in general expected to be mediated by gravitons, but there are more hypothesised mechanisms of these interactions. For example, one theory indicates a mass mixing of ordinary matter particle with its mirror partner via flavour gauge bosons. This possibility would allow neutron-mirror neutron oscillations described by the six-fermion operator [1].

3.3.2 Oscillations of Neutrons in Sterile Neutrons

A high-dimensional operator (d = 9) O is expected to give rise to the oscillations between neutrons and sterile neutrons by six-quark coupling, similarly as for the neutron-antineutron oscillations. O is approximately equal to $\frac{1}{M^5}(udd)(u^{'}d^{'}d^{'})$ where M^5 is a mass scale.

The neutron-sterile neutron ($n - n^{'}$) oscillations should be observable both in the disappearance experiment ($n \rightarrow n^{'}$) with trapped UCNs, and in the newly proposed experiments with the beam neutrons. More specifically, low-energy neutrons called cold neutrons can potentially oscillate into their sterile state as they propagate through an experimental cavity leading either to the disappearance ($n \rightarrow n^{'}$), regeneration ($n \rightarrow n^{'} \rightarrow n$) or neutron-antineutron conversion via the sterile state ($n \rightarrow n^{'} \rightarrow \bar{n}$) processes [19]. The most suitable cold neutron energy for the disappearance and regeneration experiment usually lies below 10^{-7} eV [32]. A factor that limits the sensitivity of the experiments mentioned is the magnetic field.

Namely, the problem arises from the terrestrial magnetic field with a magnitude of about 0.5 G felt by the neutrons. More specifically, the ground energy level of a neutron is raised by μB where μ is a magnetic moment of the neutron. There is no terrestrial magnetic field felt by the sterile neutron which would compensate for this effect leading to Zeeman splitting of the energy levels. Consequently, the oscillations are suppressed as the energy levels do not match precisely between the neutrons and sterile neutrons [33].

The neutron-sterile neutron oscillations violate B by one unit. However, a conserved combined B can be found if the sterile neutrons come from the mirror sector. Namely, B in the ordinary sector, where it is equal to ΔB = 1, and the mirror sector where $\Delta B^{'}$ = -1 [1]. This gives a conserved quantity ΔB + $\Delta B^{'}$ equal to 0. Conservation of the combined B indicates that such oscillations are not necessarily suppressed. In contrast, nor the ordinary world B and the combined B is conserved in the neutron-antineutron oscillations ($\Delta B^{'} = 0$ in this case) [19].

3.3.3 Mirror Dark Matter and Effect of Neutron-Mirror Neutron Oscillations on the Cosmic Rays

There is strong evidence for dark matter. The main property of dark matter which distinguishes it from ordinary matter is that it cannot interact via electromagnetic force [34]. Presence of the dark matter in the Universe manifests in several different astronomical observations. For example, in the pattern and dynamics of the large-scale structures of the Universe [35]. These structures are made of galaxies that are attracted by gravity. Their pattern resembles a spider web [36].

One of the possible candidates of dark matter is a sector of sterile particles. This sector can, in principle, be made of mirror particles since they would be sterile to the ordinary electromagnetic, weak and strong interactions. Mirror dark matter made by the duplication of the ordinary matter particles can explain the ratio of $\frac{\Omega_{DM}}{\Omega_B} \approx 5$ where Ω_{DM} and Ω_B is the dark matter and baryon density parameter, respectively. The ratio represents the relative energy density of the dark matter and ordinary matter constituents in the Universe [35]. The initial condition of the currently discussed mirror dark matter models is that the reheat temperature of the mirror sector is smaller than the temperature of the ordinary sector. It is then hypothesised by Bento and Berezhiani [37] that the B and L violating processes, which are induced in the interactions between the ordinary particles and mirror particles, including the n - $n^{'}$ oscillations, led to the baryon asymmetry (baryogenesis) both in the ordinary and mirror sectors. Such a phenomenon would be called a co-genesis and would affect the magnitude of the $\frac{\Omega_{DM}}{\Omega_B}$ ratio [38].

The neutron-sterile neutron oscillations would modify the spectrum of ultra-high-energy primary cosmic rays if the mirror world of particles exists. This could imply that sterile neutrons are equivalent to mirror neutrons [38]. Then, Greisen-

Zatsepin-Kuzmin (GZK) cutoff is predicted at 5×10^{19} eV (50 EeV) which corresponds to the energy above which the cosmic rays are expected to disappear from the spectrum provided that the ultra-high-energy cosmic rays are made dominantly of protons [39]. The reason for the disappearance is predicted by high energy protons being excited by CMB photons leading to pion and proton/neutron production. Produced neutrons can then transform into mirror neutrons. However, the GZK cutoff is expected to be at a higher energy for the mirror matter. Namely, at approximately 10×10^{19} eV (100 EeV). Therefore, neutrons produced with energy between the ordinary matter and mirror matter GZK cutoff should disappear by transformation into mirror neutrons. An interesting phenomenon occurs above the mirror matter GZK cutoff where it is hypothesised that mirror protons that make up the high energy cosmic rays can be excited by the mirror CMB photons to produce mirror protons and neutrons. These mirror neutrons can then transform into ordinary matter neutrons. Subsequently, neutrons can decay to protons and add up into the ordinary matter cosmic rays. Consequently, the ultra-high-energy cosmic ray intensity increase should be observed on the spectrum above 100 EeV. Nevertheless, experimental facilities, namely Pierre Auger Observatory [40] and Telescope Array detectors [41], do not provide enough of statistics from their measurements of the spectrum at ultra-high-energies to test whether the described ultra-high-energy processes which involve the neutron-mirror neutron oscillations take place [38].

4 The Search for Neutrons to Sterile Neutrons Conversions at the ESS

4.1 Introduction

Presently under construction, the ESS is a multidisciplinary international laboratory located in Lund, Sweden, with thirteen European member states and will become one of Europe's flagship facilities [42]. The project has been driven by the neutron scattering community. The first 15 instruments, covering a wide range of topics in neutron science, have been funded in the first call for proposals and will be brought online in the next few years. However, as defined in the ESS statutes, the scope of ESS is to build and operate 22 world-leading instruments in an open user programme [43]. During this first call of a proposal in 2015, an international collaboration submitted a request for a cold neutron beam facility (ANNI) for particle physics at the ESS. This proposal received an exceptionally high ranking, though it was not included in the first 15 instruments. The ESS analysed the capability gaps [44] later in 2018 remaining after construction of the first 15 instruments. The result of this analysis has shown that one of the communities that is most obviously not given enough attention is the particle physics community. Therefore, the ESS gave high priority to fundamental physics for the next call of instruments (16-22).

In this context, this thesis will be dedicated to the study of the ANNI beamline and its associated sterile neutron experiment HIBEAM. This work will be a part of the new call for instrument proposal that is foreseen in the next few years at the ESS.

4.2 The European Spallation Source

ESS is equipped with a powerful proton linear accelerator. The pulsed proton beam with a repetition rate of 14 Hz and pulse duration of 2.86 ms is accelerated to 2 GeV towards a target. The target is shielded by the stainless steel wall of a thickness of 3.5 m that is called a monolith. The monolith has a radius of 5.5 m and starts 2 m after the moderator centre. The proton beam with an average power of 5 MW hits the target made of tungsten placed inside a revolving disk with openings (see the target wheel in Figure 3). Each proton pulse will enter in a different opening, allowing the target to cool down. When the proton beam hits one of the openings, it penetrates through the disk and collides with the target. Consequently, spallation [45] takes place. Spallation is a two-stage process that is initiated by high-energy particles, accelerated protons, in this case, striking atomic nuclei in the target. High-energy protons, neutrons or pions are emitted

from the target in the first stage. These particles either escape from the target, or excite some of the target's nuclei. Subsequently, the excited nuclei emit low-energy protons, neutrons, or alpha particles as they relax to the ground state in the second stage. The goal at the ESS is to extract as many neutrons as possible from the spallation process. This beam of neutrons with a pulsed nature then enters a moderator, which slows down the neutrons before they reach the ESS beam ports. The beam ports, or beamline openings, extend inside the monolith from the radius of 2 m (see the position of the neutron beam extraction in Figure 3) [1, 46].

The beam ports extract the neutrons from the target. Subsequently, the neutrons are transported over a long distance to the experimental area thanks to the neutron guide. The instruments at ESS have a different length depending on the type of instrument and their scientific case [1]. An overview of the ESS instrument with the location of the ANNI and HIBEAM experiment is shown in Figure 2.

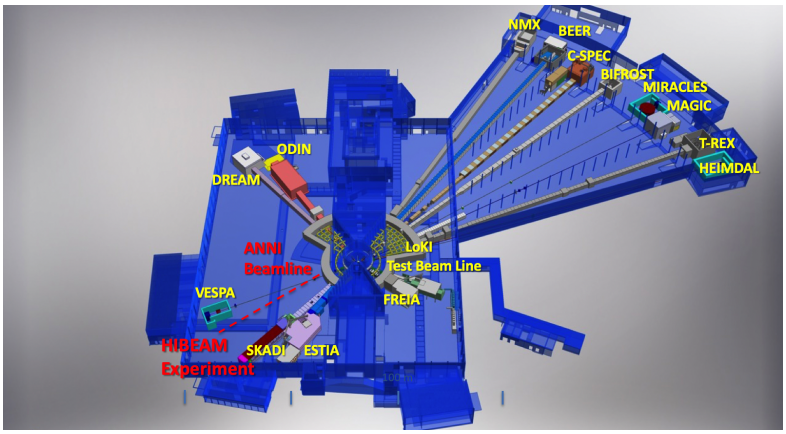

Figure 2: The ESS instruments and ANNI/HIBEAM location. Adapted from ref. 1.

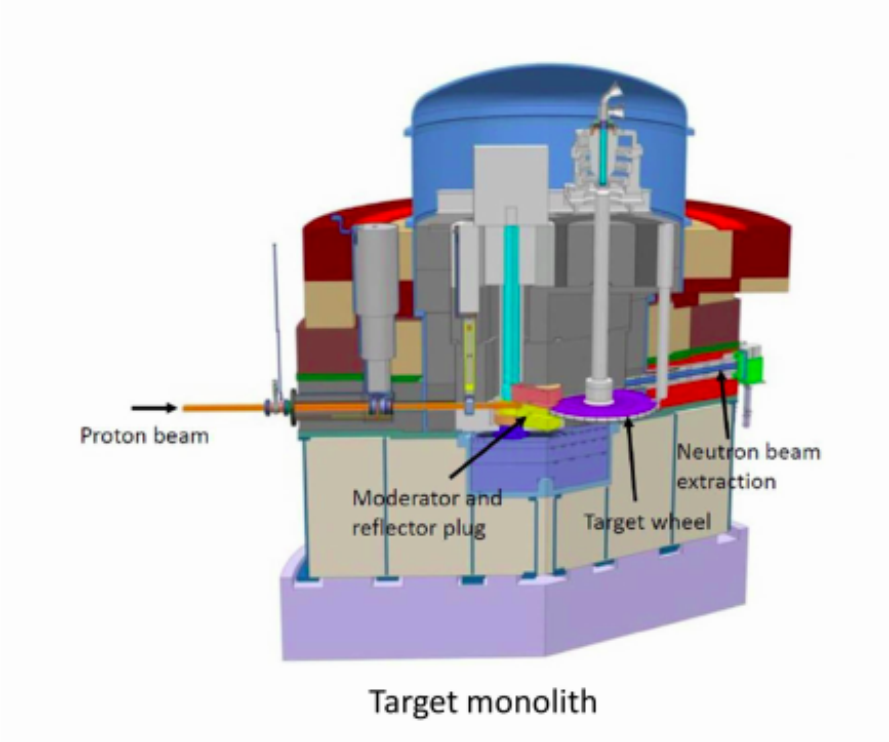

Figure 3: The cross-sectional view of the target monolith. Adapted from ref. 1.

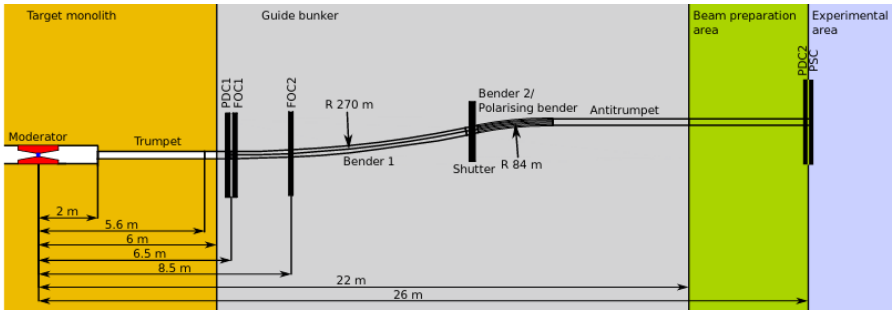

Figure 4: Overview of the ANNI beamline. Adapted from ref. 1.

4.3 The ANNI Beamline

Pulsed beams provide immense advantages for precision experiments with cold neutrons. They are used at continuous sources despite the related substantial decrease in intensity to minimise and measure systematic effects. The experiments at the ESS will benefit from the pulse structure of the source and its 50 times higher peak brightness compared to the most intense reactor facilities, making

novel concepts feasible. As a consequence, the ANNI beamline was proposed as a neutron beamline with the potential for a range of experiments (beyond the HIBEAM programme that is discussed later), including improvement in measurements in neutron beta decay of one order of magnitude in accuracy and a search for a non-zero electric dipole moment of the neutron [47]. The design from the ANNI proposal [47] is shown in Figure 4. The S-shaped guide preferentially selects cold neutrons, which are passed into an experimental area ultimately. The S-shaped guide allows to remove a part of the contribution of fast neutrons (i.e. neutrons with energy greater than 1 eV) and simultaneously keep as many low-energy (slow) neutrons as possible.

The geometry of ANNI was proposed by Soldner et al. [47]. A side-view of the geometry can be seen in Figure 4, where PDC corresponds to the pulse-defining chopper, and FOC corresponds to the frame overlap chopper. A neutron chopper is a device designed to interrupt the neutron beam for a well-defined duration periodically. They act nearly as a neutron switch that can select neutrons with a certain velocity. The length of the bender 1 and bender 2 section is 8 m and 2.5 m, respectively. There is a straight section in between bender 1 and bender 2 with a length of 0.4 m. The neutron guide of ANNI terminates at a distance of 22 m from the centre of the target monolith. The horizontal dimension of the neutron guides is bigger than the vertical one since the ESS moderator is flat [47]. There is a big experimental area, where different experimental setups can be implemented at the end of the neutron guide. The HIBEAM collaboration will design and build an experiment in this experimental area that will make use of the ANNI beam to search for the neutron to sterile neutron conversions.

4.4 The High Intensity Baryon Extraction and Measurement Experiment

The HIBEAM collaboration proposes an experiment to search for the conversion of $n \to n'$ and several other searches for sterile neutrons. These experiments will take advantage of the unique potential of the ESS.

Two main experimental approaches can be used to search for sterile neutrons: measurements of neutrons trapped in an UCN bottle and, as proposed at HIBEAM, measurements of beam neutrons. The principles behind these approaches are illustrated in Figure 5. There would be anomalous loss of neutrons from the trap via their conversion to sterile neutrons (see Figure 5a) in the case of UCN searches.

With the beam neutrons, the experiments can look for:

- the regeneration of neutrons following a beam stop (see Figure 5b),

- an unexplained disappearance of neutron flux (similar to the UCN search) (see Figure 5c),
- and the conversion process $n \to \bar{n}$ via a sterile neutron state (see Figure 5d).

With both UCN and beam of neutrons, the experiments should scan as wide a range of magnetic fields as possible to induce the neutron-sterile neutron transitions; this is due to the need to ensure degeneracy between the neutron in visible and sterile sectors. A neutron in a sterile sector may be affected by a sterile magnetic field $\mathbf{B}'$. Such a magnetic field can be generated by hypothetical ionization and flow of gravitationally captured dark material in and around the Earth [48]. Such an accumulation could occur due to ionized gas clouds of sterile atoms captured by the Earth, e.g. due to the photon-sterile photon kinetic mixing; present experimental and cosmological limits on such mixing [49] and geophysical limits [50] still allow the presence of a relevant amount of sterile material at the Earth [48]. The presence of this sterile magnetic field $\mathbf{B}'$ and the laboratory magnetic field $\mathbf{B}$ create a difference in the potential energy of a neutron in the visible sector and a sterile neutron in the sterile world. This energy difference suppresses the transformation unless $\mathbf{B} \sim \mathbf{B}'$ [48] as was discussed in Section 3.3.2. This can manifest itself when varying $\mathbf{B}$ over the unknown range of $\mathbf{B}'$ in an experiment giving the resonance value when $\mathbf{B} \sim \mathbf{B}'$ at which the probability of is greatly enhanced [1].

Several dedicated experiments searching for $n \to n'$ processes with UCN were performed in the last decade [51–58]. The interpretations and limits for the UCN measurements rely on the experimental assumptions, which may be poorly understood for neutron collisions on UCN material trap walls [59]. This source of systematic uncertainty can be removed by performing dedicated searches with propagating cold neutron beam in a magnetic field, as planned for HIBEAM.

It is important to note that the lower the neutron's energy, the longer is its propagation time, giving a higher probability for the oscillation. Consequently, cold neutrons are demanded in all the experiments. The $n \to n'$ disappearance experiment (see Figure 5c) will involve a current-integrating beam detector labelled by M to measure the neutron flux at the end of the guide in the entrance of the experimental area. The experimental area corresponds to the location where the neutrons are let to propagate inside the vacuum pipe without a guide. The second detector labelled by C, a current-integrating beam detector, is located in the end of the vacuum pipe. The C detector absorbs the beam with much higher neutron counting efficiency than the M detector. The ratio between neutron fluxes at the M and C detectors reveals possible neutron disappearance. This experiment assumes that there is a constant mirror magnetic field $\mathbf{B}'$ present in the overall flight length of the neutrons. It is expected that the neutron oscillations are

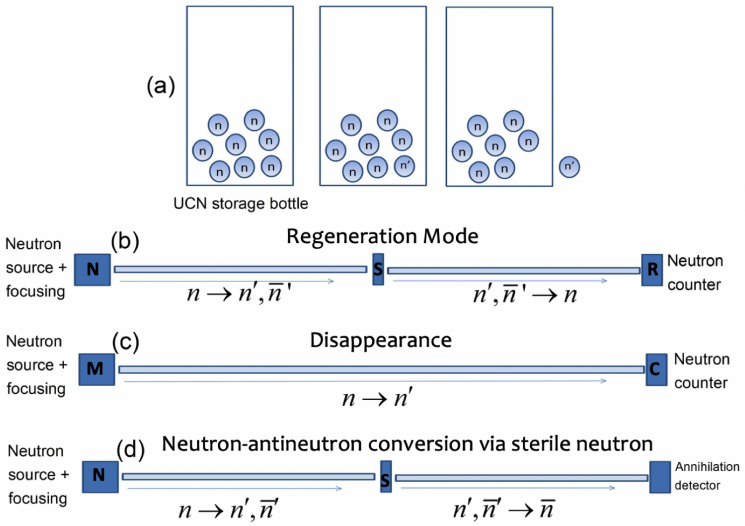

Figure 5: The illustration of the principles of searches for sterile neutron oscillation. In the UCN trap (a), it is possible that neutrons effectively disappear, possibly lowering the measured values of the neutron lifetime. For neutron beams, both regeneration (b) ($n \to [n', \bar{n}'] \to n$) and disappearance (c) ($n \to n', \bar{n}'$) search modes are possible. Another possibility (d) is regenerative in style, though instead leads to further mixing to an antineutron ($n \to \{n', \bar{n}'\} \to \bar{n}$), requiring an annihilation detector. For the regeneration and neutron-antineutron conversion searches, a neutron absorber must be placed at the halfway point of the beamline, preventing all ordinary neutrons from proceeding through the experimental cavity while permitting sterile species to pass unencumbered. The figure was adapted from ref. 1.

magnified when $\mathbf{B}'$ is matched by the artificially induced magnetic field B inside the vacuum pipe. $\mathbf{B}$ will be varied between -0.5 G and 0.5 G. A lower limit on $\tau_{nn'}$ by disappearance can be estimated based on the measurements [1]. A sensitivity of the experiment (the lower limit on $\tau_{nn'}$) increases with the flight path L of the neutron and $\sqrt[4]{T}$, where T is a duration of a single measurement assuming that the incoming neutron flux is constant. Increasing L can be challenging due to the space limitations of a research facility [60]. Figure 6 shows the current limits from UCN-based experiments together with the expected sensitivity of the HIBEAM experiment (in the disappearance mode) after a one-year ESS run for the power usage of 1 MW. Increases in disappearance sensitivity of greater than an order of magnitude are possible depending on the value of the magnetic field used. It can be seen that HIBEAM covers a wide range of oscillation times for a given magnetic field value (up to and beyond an order of magnitude), many of which are unexplored by UCN-based experiments, and remain free of the model assumptions of those searches.

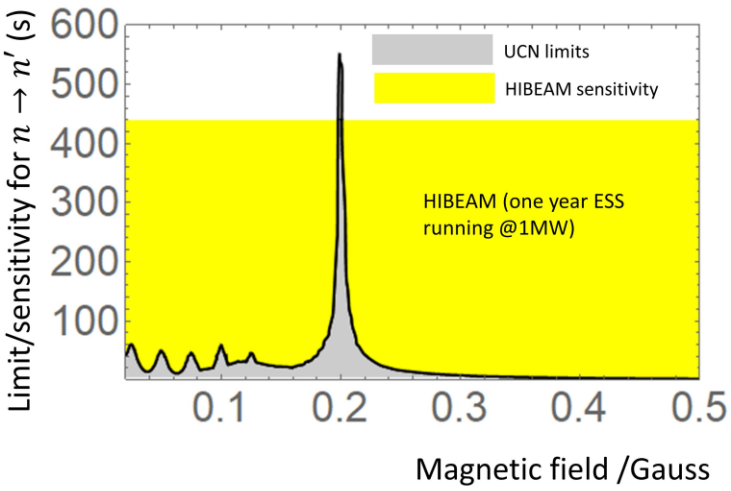

Figure 6: The black line describes the excluded neutron oscillation times (τ_s) for $n \to n'$ disappearance from UCN experiments as a function of the magnetic field $\mathbf{B}'$. The projected sensitivity for HIBEAM for the disappearance experiment is also shown in yellow for one year's run at the ESS assuming a power of 1MW. Adapted from ref. 1.

The $n \to n'$ regeneration experiment is similar to the previous disappearance experiment, but two consecutive independent oscillations must happen. The probability for the signal event will decrease quadratically as a consequence. There will be a current-integrating neutron beam detector at the entrance of the experimen-

tal area labelled by N. Then, a neutron absorber S in the middle of the vacuum pipe will stop all the neutrons that did not undertake the regeneration process before they reach the R detector. At the end of the vacuum pipe, another current-integrating neutron beam detector labelled by R will detect the neutrons that converted to sterile neutrons. There is a need for a highly efficient R detector since the signal is estimated to be small. The sensitivity of this experiment increases with $\sqrt{L_1 L_2}$, where L_1 is a flight path between the N detector and the S absorber, and L_2 is a flight path between the S absorber and the R detector. The sensitivity also increases with $\sqrt[8]{T}$. The best choice is to keep $L_1 = L_2$ if the total L of this experiment is constant [60]. Finally, the $n \to (n', \bar{n'}) \to \bar{n}$ experiment requires a similar set-up as for the $n \to \bar{n}$ experiment planned for NNBAR. The reason is that the final state will be an antineutron, and in order to detect such particle, an annihilation detector is required. The signature of the neutron-antineutron transition is via the annihilation of the antineutron on a Carbon target surrounded by the annihilation detector (see Figure 5d). Such interactions produce a multipion state (3-5 charged pions and photons from neutral pion decays) with momenta between 100 and 300 MeV [61, 62].

5 Background and Shielding Studies for the HIBEAM Experiment

As stated previously, the sensitivity of the sterile neutron searches depends on the background rates. Several components contribute to the background: the spallation background (i.e. neutrons and photons coming directly from the target), the secondary particles produced by the neutrons and gammas that escape from the target, and the cosmic background produced by particles formed by the interactions of the primary cosmic rays with the Earth's atmosphere [1, 63]. The study of the spallation background and the shielding design of the ANNI beamline are the primary objectives of this work. All the calculations shown in this thesis aim to estimate the background contribution at the exit of the ANNI neutron guide at 22 m (see section 4.3), where the neutrons are transmitted to the experimental area and to estimate the thickness of the shielding needed from the last part of the ANNI beamline.

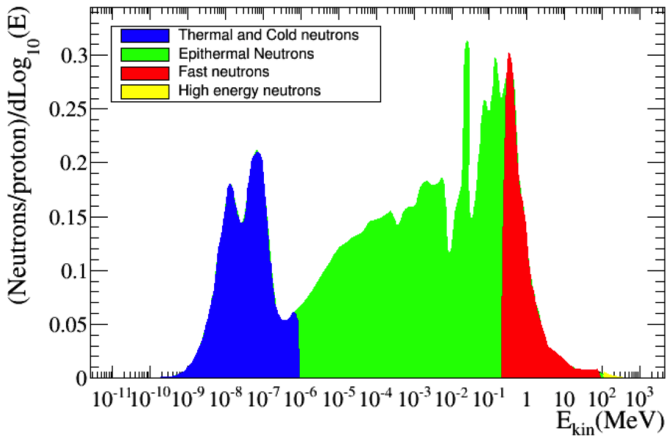

Figure 7: The ESS spallation spectrum at 2 m. The spectrum was averaged on all the beamports. Adapted from ref. 64.

The spallation neutron spectrum extends up to the energies of protons that were accelerated to collide with the target as illustrated in Figure 7 [64]. Therefore, there is a significant fraction of epithermal and fast neutrons present. These neutrons do not reach the moderator, and consequently, they are not moderated. However, they are still able to enter the beamline. Therefore, they contribute to the background significantly and generate a shower of secondary particles that may

be difficult to shield. Simultaneously, the radiation of neutrons is a threat to living organisms considering the radiological protection, and they must be shielded [63]. A straightforward solution to suppress the fast neutron and photon background is to use a curved guide section called a bender, as proposed for ANNI. Most of the fast neutrons and photons will travel straight, while the cold neutrons will be transported inside the curved guide [1, 63]. The fast neutrons and photons will be later absorbed by the shielding material [65].

Another important aspect that must be taken into account is the radiological requirement that needs to be satisfied to fulfil the laws to operate the beamline at ESS [66]. The effective dose H $[Sv]$ quantifies a threat of a radiation on a living organism. H with SI units of $[J/kg]$ scales with the type and energy of particles that make the radiation as well as the type of an irradiated tissue. Conversion factors at a given energy allow calculating H by multiplying it with the flux of neutrons. The dependence of conversion factors on energy of neutrons can be seen in Figure 8 [65]. These conversion factors were computed for the irradiation of a human body by Muhrer et al. [67], and are listed in an internal ESS document. As described previously, the ESS target is shielded by a stainless steel wall called the monolith and further away by another structure called the bunker (located 15 m away from the center of target monolith) that provides additional shielding. Furthermore, every beamline at ESS needs additional shielding around the guide after crossing the bunker wall. The radiation requirement is that the maximal acceptable dose rate of both neutrons and photons at the surface of the shielding should be < 3 μSv/h [1]. An additional safety factor of 2 is added for the Monte Carlo simulation, and therefore the requirement for the simulation is set to 1.5 μSv/h [68].

Neutrons represent the most dangerous radiation which is produced at ESS because of their high penetrability in shielding materials. Especially, fast neutrons are difficult to be absorbed. The reason is that the neutrons do not possess an electric charge, and thus their ability to interact with shielding material is limited compared to charged particles. This also applies to photons, another dangerous source of radiation produced in the spallation process at ESS.

Both the shielding effectiveness and the background simulations in this work were performed using a Monte Carlo radiation transport code named PHITS that is described in the next section.

6 Methodology

6.1 Particle and Heavy Ion Transport code System

The spallation process and a subsequent propagation of its products, including neutrons, through the ESS monolith and ANNI beamline is simulated using PHITS.

PHITS is based on Monte Carlo simulation that provides statistical method to transport particles such as neutrons or photons and ionized atoms. The upper energy limit of particle or nucleon inside an atom that can be transported by PHITS is 1 TeV. PHITS finds application in designing radiological protection, estimating background at any point of a neutron guiding system, or simulating boron neutron capture cancer therapy [4, 69].

PHITS allows taking measurements of various quantities in a simulation using virtual detectors called tallies. The quantities of interest in this project are the neutron flux and the dose rates . The T - Cross tally measures both the current and flux through a surface defined by intersection of two geometrical regions also called cells in PHITS (see Figure 9). The flux is simply the number of neutrons/cm$^2 \times s$. The T - Point is another example of a tally, which measures the flux only. It is a point-like detector made of an imaginary sphere with a radius of 1 cm. The standard deviation, which equals to the error of all the measurements performed by a tally in a given bin, is estimated with Equation 2 where N is the total number of measurements, x_i and w_i corresponds to the value of a single measurement and a weight of the measurement, respectively, and $\bar{x}$ and $\bar{w}$ corresponds to the average over all the measurements and weights, respectively.

$$\sigma = \sqrt{\frac{\sum_{j=1}^{N}(\frac{x_j w_j}{\bar{w}})^2 - N\bar{x}^2}{N(N-1)}} \tag{2}$$

The flux measured over a defined range of energies is sometimes referred as a spectrum. It is conventional to divide the y-axis of the spectrum by a lethargy. The range of energies depicted on the x-axis is divided into bins in PHITS. Lethargy is then given by $\ln(\frac{E_{max}}{E_{min}})$, where E_{max} and E_{min} is the maximal and minimal energy of the energy bin, respectively [70].

PHITS supports the open-mpi library [71], allowing increasing the number of simulated events in a given time interval significantly. As a consequence, the statistics of measurements are improved substantially. In the other words, variance of measurements is reduced. The ESS computer cluster is used as a main resource for the parallel computing in this project. The computer cluster at ESS is made of a set of nodes, that can work together on a single simulation. Each node consists of many central processing unit (CPU) cores or hardware threads, sometimes referred as processing units. For example, 320 processing units from 10 nodes are involved in total for the most demanding simulations in this project. A concept of batch number is introduced in PHITS. This concept is related to the parallel computing since the number of batches is automatically adjusted by PHITS to be equal to (n_{PU} - 1) where n_{PU} is the number of processing units. In principle, an individual simulation is run in each batch. A number of particles generated by a source is fixed for all the batches. The observables are estimated and reported by tallies

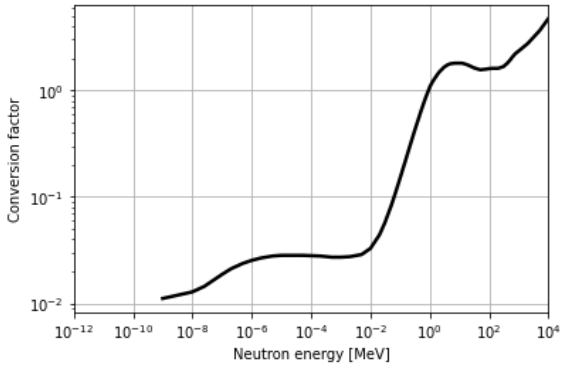

Figure 8: A logarithmic interpolated data points of conversion factors vs energy of neutrons [67].

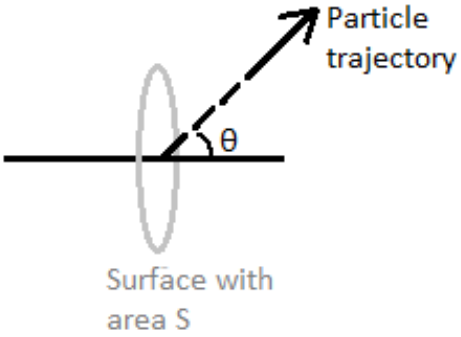

Figure 9: The sketch of a particle passing through the surface with area S at angle θ.

after all the events in the batch are simulated. In the end, observable estimates and their error estimates from all the batches are combined into the final estimate using weighted summations in Equation 3 and Equation 4, respectively, where A is a multiplication factor, N is the number of observable estimates, x_i is a value of observable estimate i, w_i is a weight of the observable estimate i, w is a sum over all the weights w_i, and σ_{x_i} is an error of x_i. The weight is set to be one when combining the estimates in the case of equal number of events in each batch. The advantage of setting a large batch number, which is even greater than the number of processing units, is that interim results of observable estimates are reported frequently during the simulation, but at the cost of an increased processing time [70].

The fact that observable estimates can be combined using Equation 3 and Equation 4 can be used to improve statistics by combining observable estimates from independent measurements. This method was used to obtain spectrum of neutrons at 22 m, which required a large number of simulated events. The weight was set to one provided that the number of batches and simulated events in each batch was equal. Otherwise, an appropriate weight for each observable estimate was required to be set. The independence of each observable estimate was reached by modifying the initial random number labelled by "rseed" of the simulation. Then, PHITS generated random number labelled by "rijk" for each batch according to rseed.

In addition, the combination of observable estimates can be used to attain parallel computing on a consumer computer, when open-mpi libraries are not available, or not compatible with installed PHITS version. This method was used mainly for source term simulations which are less computationally demanding in this project. PHITS without open-mpi libraries uses a single processing unit for a simulation. Then, it is possible to run multiple simulations according to the

number of available CPU cores on the computer and then combine the observable estimates according to Equation 3 and Equation 4, again provided that the observable estimates are independent.

$$\bar{x} = A \sum_{i=1}^{N} \frac{w_i}{w} x_i \tag{3}$$

$$\bar{\sigma_x} = A \sqrt{\sum_{i=1}^{N} \frac{w_i^2}{w^2} \sigma_{x_i}^2} \tag{4}$$

6.2 The ANNI Beamline Geometry

In order to calculate the background contributions and the radiation dose rates, it was necessary to implement a detailed model of the ESS target and the ANNI beamline. The ANNI beamline geometric model was implemented in this project expanding the official ESS target model. The PHITS model in comparison with the engineering model [72] is depicted in Figure 10. The relative position of the moderator and the ANNI opening can be seen in Figure 11. The model is highly detailed and contains all the relevant components that contribute to the background. The geometric model of ANNI was created based on Figure 4 using CombLayer [73]. CombLayer is a set of C++ scripts and libraries that allow producing a complex geometrical model for several neutron transport simulations including PHITS. The input to CombLayer is written in C++ where all the objects in the model of a beamline and their relative positions are defined by means of object-oriented programming.

The side view of the geometric model of ANNI beamline created in CombLayer can be seen in Figure 12. The opening of the ANNI beamline was at x = 2 m, where x was a horizontal distance from the moderator center. There was a neutron guide (black line in Figure 12) which extended from x = 2 m to x = 22 m. The most general purpose of the neutron guide is to transport cold neutrons with a minimal loss. Its inner wall is usually covered by a thin, highly reflective material. This thin layer of the reflective material, a neutron mirror, is deposited on a substrate material. There is a limiting factor of a single layer mirror for neutrons to be reflected given by the critical angle that can be calculated from Snell's law [74]. Therefore, mirrors with multiple layers are usually used. They are, in general, composed of materials with alternating high and low indexes of refraction leading to periodic interfaces. The interfaces are boundaries between the layers of a small and high index of refraction. The neutrons which encounter one of the interfaces are either reflected or transmitted. The transmitted neutrons encounter later another interface deeper in the mirror. The wave functions of

reflected neutrons which interfere constructively at the surface of the multilayer mirror then propagate further through the neutron guide. Bragg's law can be used to estimate the wavelength of reflected neutrons. The problem is that these multilayer mirrors are capable of reflecting neutrons in a narrow wavelength band only. Hence, the supermirrors [75] are used to reflect the neutrons with a wider range of wavelengths. That is accomplished by layers with varying thickness in the supermirror such that neutrons with different wavelengths are reflected.

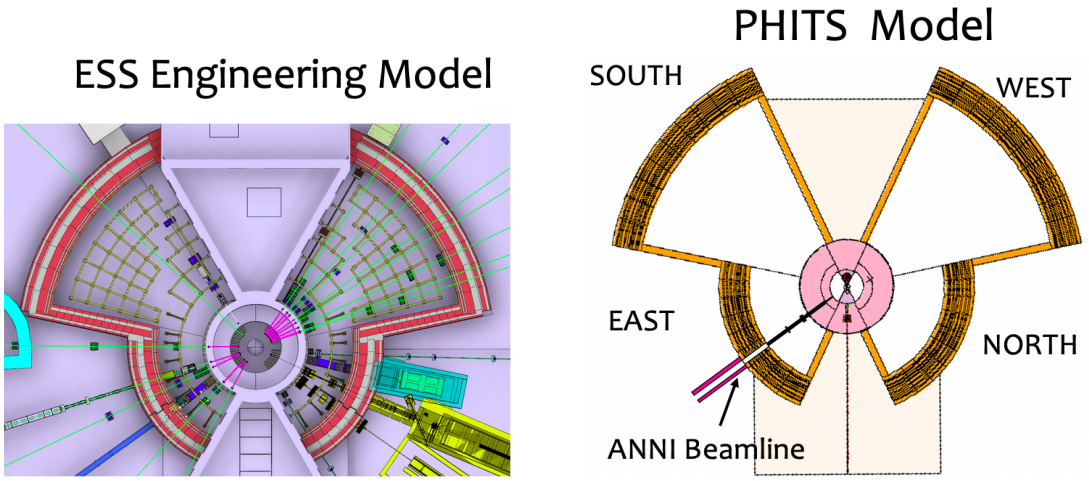

(a) Adapted from ref. 72. (b)

Figure 10: Overview of the ESS target, monolith, bunker and beamline. The ESS instruments are distributed in 4 different sectors. The ANNI beamline is located in the East sector at the beamport 5. The engineering drawing in Figure 10a shows the layout of the instruments at ESS. The corresponding PHITS model is depicted in Figure 10b, including the top view of the geometric model of the ANNI beamline.

Then, there was a vacuum pipe, which surrounded the guide, to provide the vacuum. Consequently, a beam of neutrons could propagate freely and unpolluted through the guide. The neutron guide was not surrounded by the vacuum pipe inside the monolith since the monolith provided its own vacuum system. Another important neutron optics element used was a chopper. The chopper, in general, allows controlling the properties of a neutron beam. It is made of a rotating disk, also called a blade, with two slits placed on the opposite sides of the disk such that the beam can pass through the disk only when one of the slits aligns with the guide. The chopper is called to be in an "open" position in this case. The choppers were also proposed for the ANNI beamline due to a pulsed nature of the ESS neutron source. Namely, the ANNI geometric model consisted of the PDC and

two FOCs [47]. The PDC chopper was made of two counter-rotating disks. The disks can, in principle, rotate at different frequencies. Namely, the frequency of each disk can be set to a multiple of a base frequency. The planned base frequency is 14 Hz in the case of ANNI. The combination of the disk frequencies determines the duration of output neutron pulse [76]. The responsibility of the FOCs is to keep neutron pulses separated such that frame overlap is avoided. More specifically, the frame overlap of pulses can occur since velocities vary among neutrons in a pulse. This leads to slow neutrons lagging behind the faster neutrons leading to the mixing of neutrons from different pulses [47].

The purpose of this project was to estimate the background produced by fast neutrons in the worst possible scenario, when the flux of neutrons was maximal considering the neutron beam propagating out of the bunker at x = 15 m. Therefore, all the choppers were set to be in the open position in this geometric model. The thickness of the shielding of the last part of the guide, between the bunker wall edge at x = 15 m and x = 22 m where the ANNI beamline terminates, was varied and studied in this project. The shielding thickness was initially set to be 40 cm of concrete, and its effectiveness was tested in this project. A detector was placed at x = 22 m in the central part of the beamline to measure the spectrum of neutrons and estimate the background level.

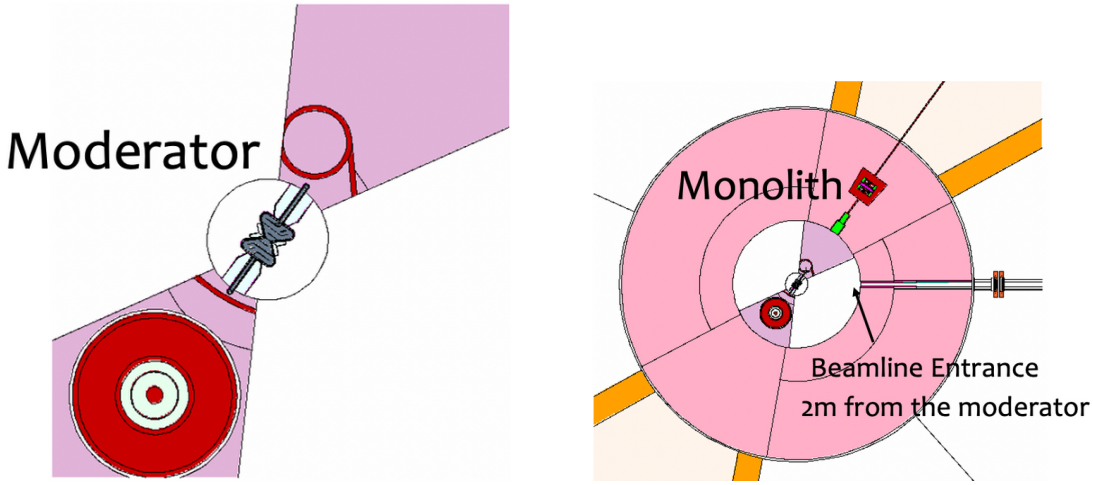

(a) (b)

Figure 11: The top view of the ESS butterfly moderator is depicted in Figure 11a. The top view of the target monolith with the ANNI beamline entrance is depicted in Figure 11b.

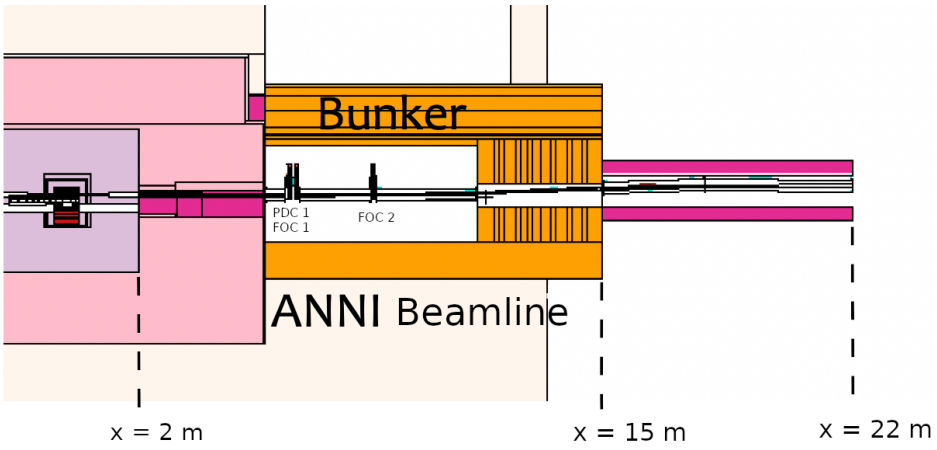

Figure 12: The side view of the geometric model created for the ANNI beamline.

6.3 Source Term

The transportation of neutrons over long distances represents a challenge for every radiation transport code. This project involved highly computationally demanding simulations due to a necessity to plot dose maps outside the bunker, more than 15 m away from the spallation source of neutrons, and a spectrum of neutrons at the end of the ANNI beamline at 22 m. A way to address this challenge was to implement a 2-step calculation method, where a source term was generated in the first step and later used as input to the simulation in the second step. This methodology was used to improve statistics of observables at such large distances from the spallation source of neutrons given the limited computational resources.

A source term was generated in the first step by measuring the flux of neutrons through a surface, usually located at a beamline opening, to get their energy distribution with respect to the angle at which they left the surface. This distribution could be then used to define a new virtual source term at the position of the surface. This procedure removed the necessity to simulate the spallation process. Consequently, the computational time for a given number of events decreased [65]. In addition, the spectrum of a new source term was reduced to neutrons that come out at a small angle θ relative to the surface normal. In fact, it was found that neutrons with $\theta < 1°$ were only relevant to observables measured outside the target monolith [77]. There are two different source terms used in this project. The first official ESS source term was adapted from Santoro et al. [77] from the test beamline. This source term had a rectangular shape with a width of 8 cm and height of 5 cm, and it was re-scaled to the dimensions of the ANNI opening

with the width and height of 9 cm and 6 cm, respectively. Each source term defined inside the ANNI beamline must be normalised such that it provides an equal number of neutrons per second at a given position, as in the case when there is a proton current of 2.5 mA hitting the target in the target monolith. The ESS source term normalisation factor was provided to be 5.87 $\times 10^{12}$ for $0° < \theta < 3°$ and was re-scaled by a factor of $\frac{9\times6}{8\times5}$ to account for the ANNI beamline opening. Then, the normalization factor was 7.98×10^{12}. The energy distribution used in this source term was defined in three intervals of θ (for θ definition see Figure 9). Namely, between θ equal to $0-1°$, $1° - 2°$, and $2° - 3°$.

The second source term was produced in this project to account for the difference in neutron energy spectrum measured through the ANNI and test beamline openings. This difference can stem from the orientation of ANNI beamline with respect to the moderator as compared to test beamline. In addition, the process of production of the source term allows studying the angular distribution of neutrons passing through the ANNI opening more thoroughly. The production of the source term started with measuring the flux of neutrons with $\theta < 3°$ through a surface defined as the intersection of the moderator with the ANNI opening at a distance of 2 m from the target (see Figure 11). More specifically, the neutron spectrum was measured for θ between $0° - 1.5°$ and $1.5° - 3°$ as a compromise between the angular resolution and magnitude of the neutron flux error [77]. The normalization factor used was the same as for the test beamline source term, $7.98 \times 10^{12}\ n/cm^2 \times s$. The energy distributions for different intervals of θ can be seen in Figure 13. The contribution of fast neutrons increased at higher θ as expected since these neutrons had less probability of reaching the moderator, where they could be slowed down. This source term was used later for the results shown in Section 7.3.

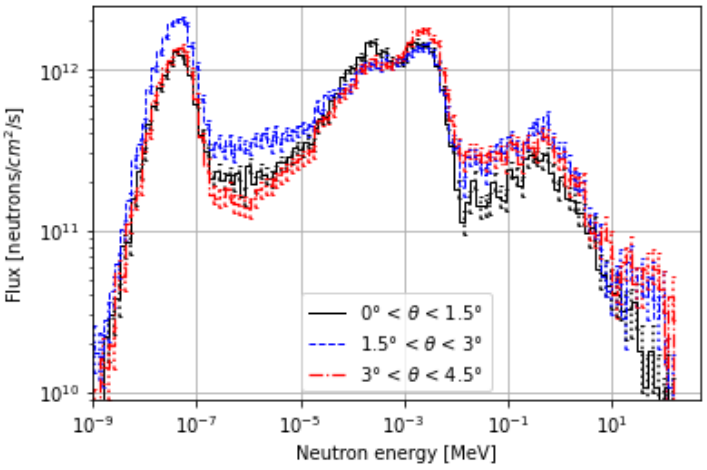

Figure 13: The comparison of the flux of neutrons arriving with different θ to the surface of the ANNI beamline opening. The contribution of fast neutrons increased when θ is above 3°.

7 Results

Initially, the simulations were performed using the proton source, simulating the spallation process and the moderation process. Then, the produced neutrons enter the ANNI beamline and subsequently, the dose rate and neutron spectrum could be studied. The simulations with run from proton suffer of lack of statistics, and for this reason the source term described above has been used to improve the quality of the calculations. The results of simulations for different source terms are described in the following sections.

7.1 Simulations with the ESS Proton Source Term

The first step in understanding the background and the dose rates for a neutron beam line is to calculate the flux of neutrons at the beamline entrance located at 2 m from the moderator (see Figure 14). This spectrum was recorded for the neutrons with $0 < \cos(\theta) < 1$. The contribution of fast neutrons to the effective dose is much higher than the contribution of slow neutrons as it is apparent from Figure 8.

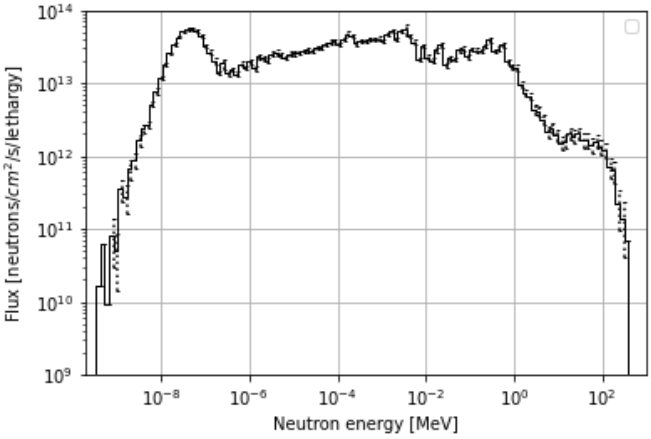

Figure 14: The flux of neutrons vs neutrons energy through the ANNI opening at 2 m from the moderator. Depicted based on the simulation with 18 millions of events.

This plot confirmed that neutrons with different energies produced in the spallation process traveled inside the ANNI beamline. Some of the neutrons leaked throughout the monolith wall as can be seen in the flux map shown in Figure 16a. The relative error on this observable is depicted in Figure 16b. It can be seen from the plot that a significant fraction of neutrons left the ANNI beamline in the bent section. Not many neutrons were observed further away from the bunker wall located at x = 15 m due to the problem of propagating the neutrons over long distance.

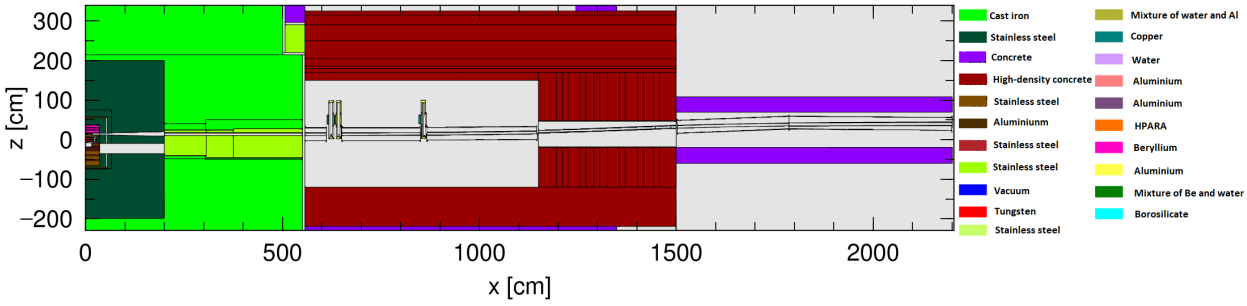

Figure 15: The side view of the ANNI beamline. The target, monolith, bunker area and the area outside the bunker is shown. Each colour represents a different material.

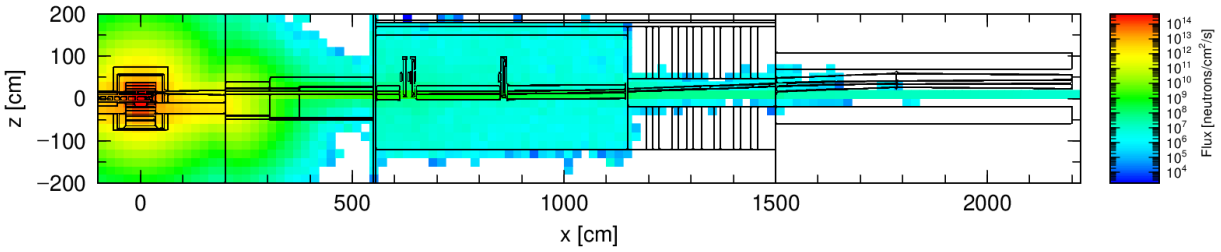

(a)

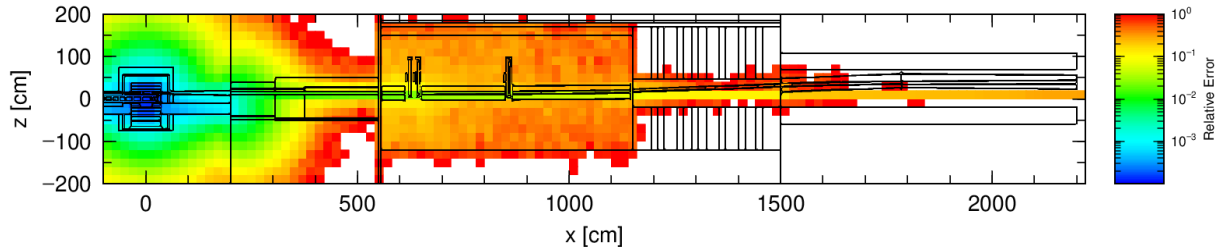

(b)

Figure 16: Integrated flux of neutrons at the different positions in the ESS target monolith and the ANNI beamline is shown in Figure 16a. Depicted based on the simulation with 18 millions of events and the ESS proton source term. A corresponding relative error on the integrated flux of neutrons is shown in Figure 16b.

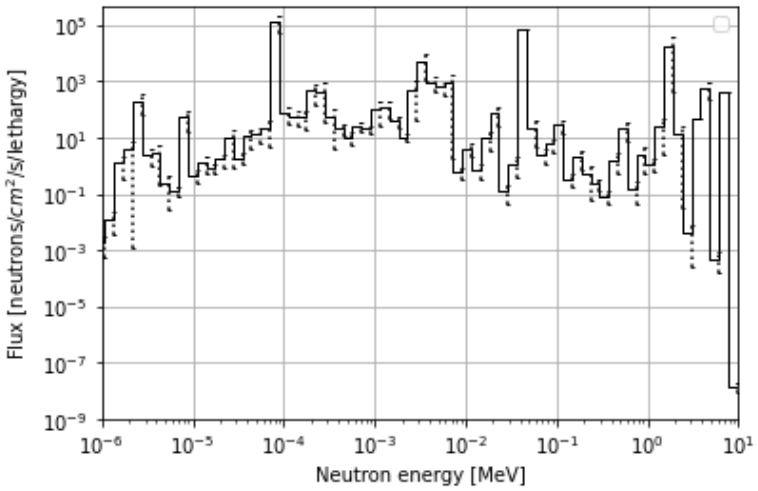

Figure 17: The flux of neutrons at x = 22 m measured in the central part of the beamline for the case of the ESS proton source term. Depicted based on the simulation with 60 millions of events.

In addition to the flux maps, a measurement of the neutron spectrum at 22 m

from the target was performed. The final neutron spectrum can be seen in Figure 17. The shape of the spectrum is in general wobbly indicating a higher relative error on the readings than in the case of spectrum at 2 m (see Figure 14), again this is due to the challenge of a simulation performed with a proton source term.

7.2 Simulations with the ESS Test Beamline Neutron Source Term

The ESS test beam line neutron source term was defined at the entrance of the ANNI beamline, and was used in the following calculations. The reason was to improve the statistics of the observables in the region outside the bunker wall (x > 15 m).

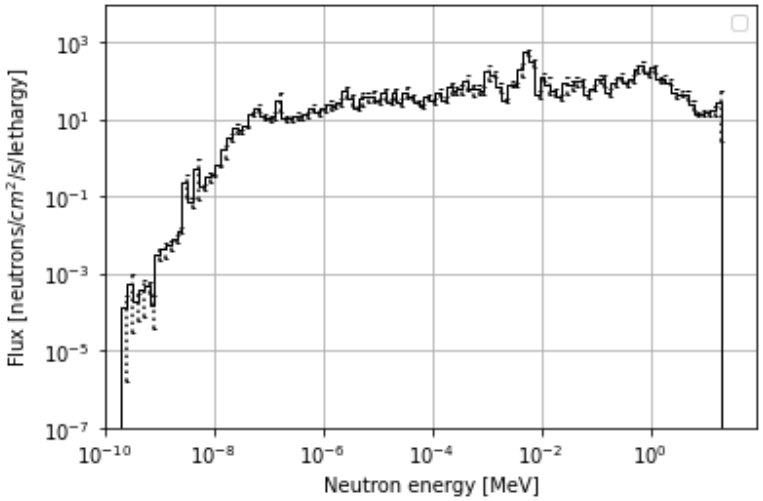

Figure 18: The flux of neutrons at 22 m from the target (x = 22 m) using the ESS test beamline neutron source term. Depicted based on the simulation with 90 millions of events.

The spectrum of neutrons at the end of ANNI beamline at x = 22 m was recorded again (see Figure 18) using the ESS test beamline neutron source term. The appearance of the spectrum was smoother in comparison to Figure 17 indicating that the magnitude of error reduced significantly. The computational time for the simulation also reduced significantly allowing to make measurements based on a higher number of events.

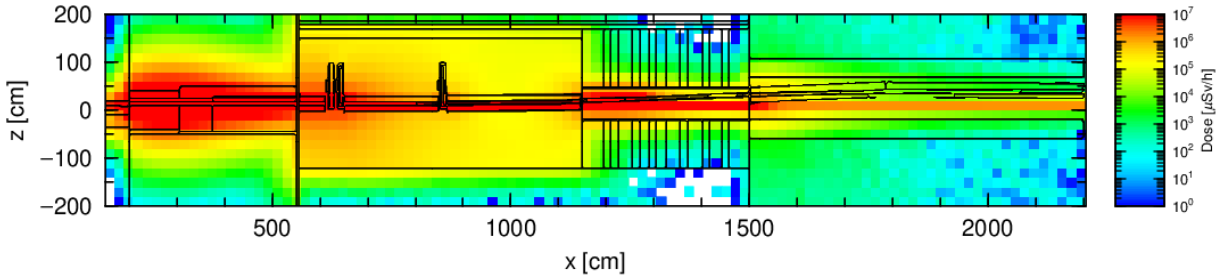

(a)

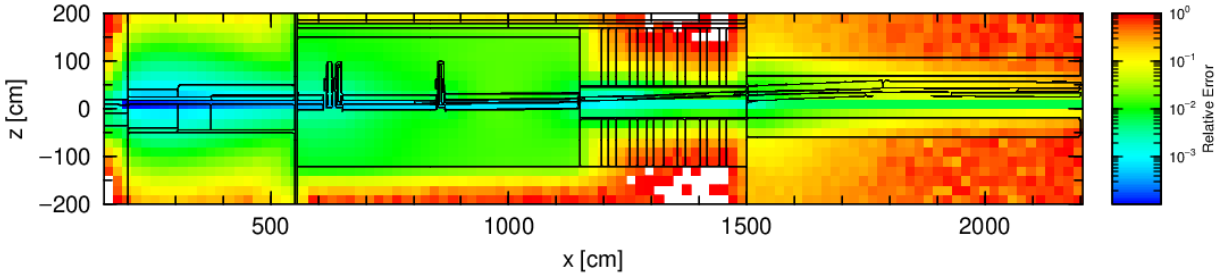

(b)

Figure 19: The dose map of neutrons for 40 cm concrete shielding of ANNI outside the bunker wall between 15 and 22 m is shown in Figure 19a. The relative error for the dose map is shown in Figure 19b. Depicted based on the simulation with 1500 millions of events. The ESS test beamline source term defined at 2 m was used. The view on ANNI is from the side.

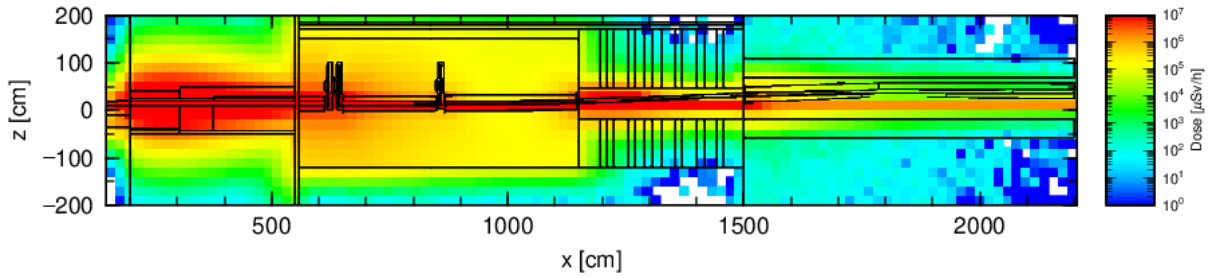

(a)

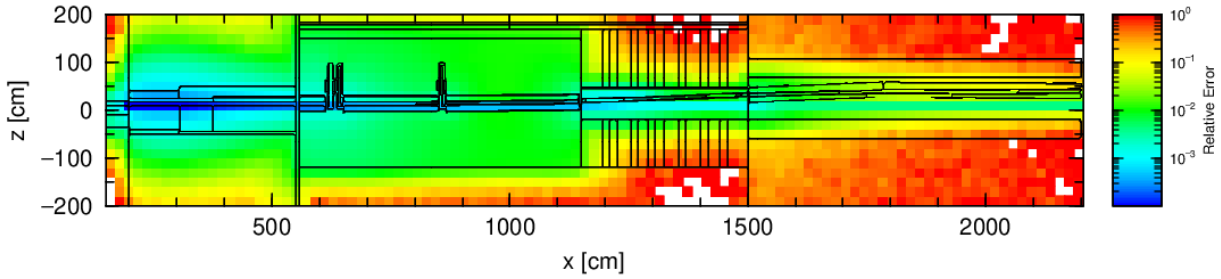

(b)

Figure 20: The dose map of neutrons for 40 cm heavy concrete shielding of ANNI outside the bunker wall between 15 and 22 m is shown in Figure 20a. The relative error for the dose map is shown in Figure 20b. Depicted based on the simulation with 1500 millions of events. The ESS test beamline source term defined at 2 m was used. The view on ANNI is from the side.

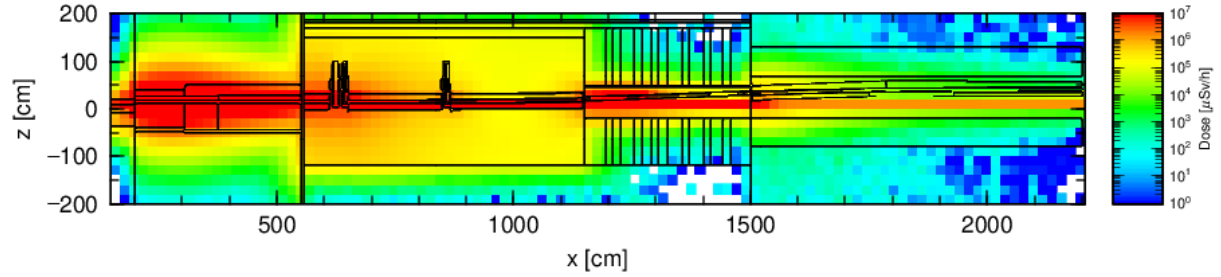

(a)

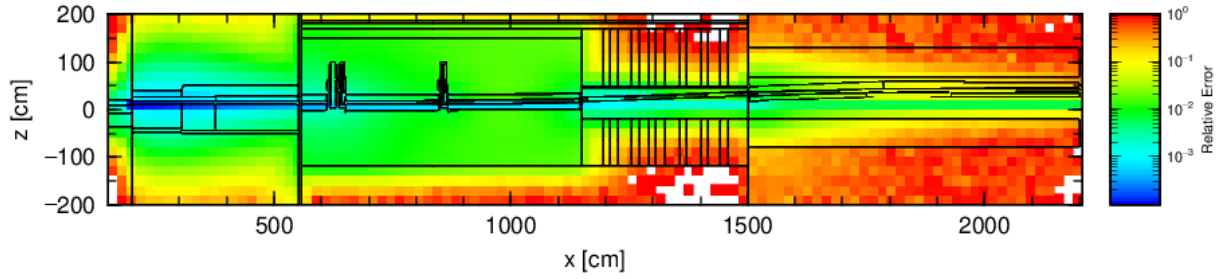

(b)

Figure 21: The dose map of neutrons for 60 cm concrete shielding of ANNI outside the bunker wall between 15 and 22 m is shown in Figure 21a. The relative error for the dose map is shown in Figure 21b. Depicted based on the simulation with 1500 millions of events. The ESS test beamline source term defined at 2 m was used. The view on ANNI is from the side.

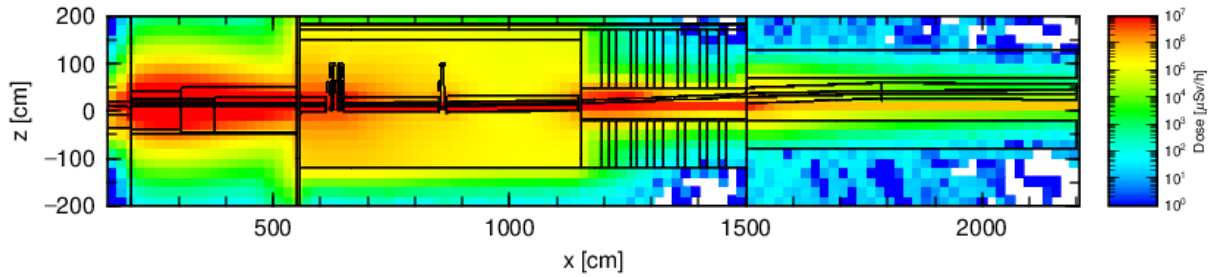

(a)

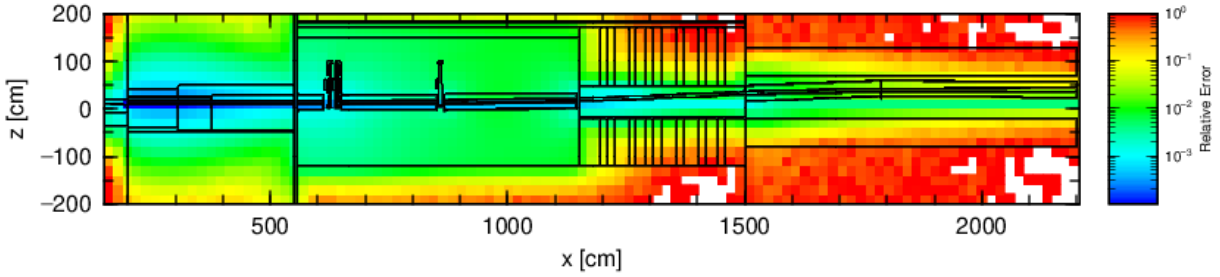

(b)

Figure 22: The dose map of neutrons for 60 cm heavy concrete shielding of ANNI outside the bunker wall between 15 and 22 m is shown in Figure 22a. The relative error for the dose map is shown in Figure 22b. Depicted based on the simulation with 1500 millions of events. The ESS test beamline source term defined at 2 m was used. The view on ANNI is from the side.

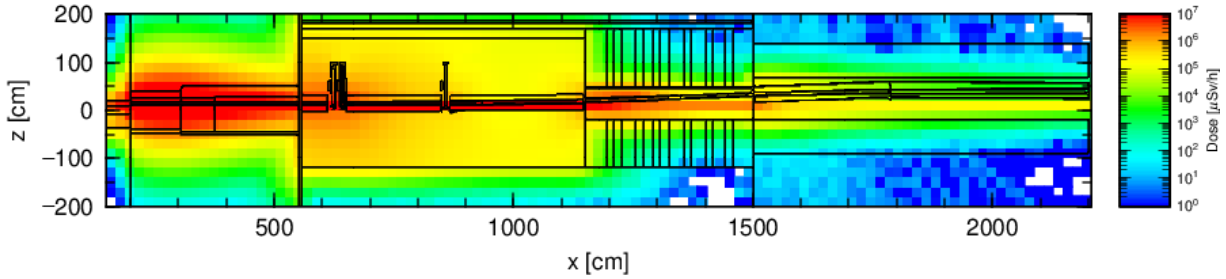

(a)

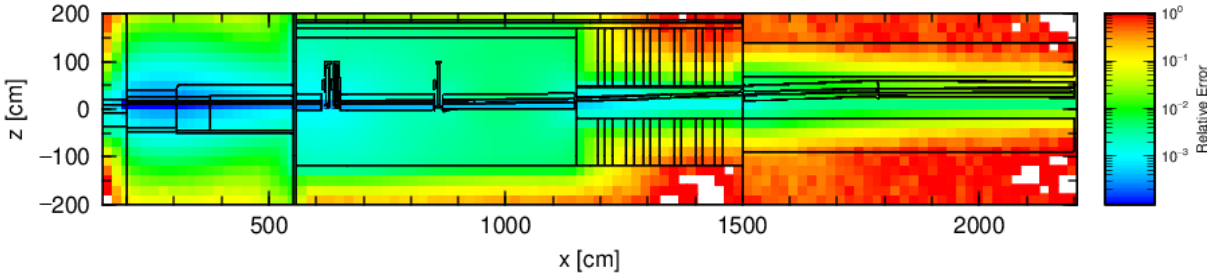

(b)

Figure 23: The dose map of neutrons for 70 cm heavy concrete shielding of ANNI outside the bunker wall between 15 and 22 m is shown in Figure 23a. The relative error for the dose map is shown in Figure 23b. Depicted based on the simulation with 1500 millions of events. The ESS test beamline source term defined at 2 m was used. The view on ANNI is from the side.

The radiation dose for neutrons for the region outside the bunker wall was also computed. The shielding thickness around the ANNI beamline was varied from 40 cm to 60 cm for both the case when the concrete and heavy concrete was used as the shielding material. Moreover, the dose map for the 70 cm thick shielding material made of the heavy concrete was calculated. Figures 19, 20, 21, 22, 23 show the radiation dose maps for the different thicknesses and their relative error at each point of the map, respectively (see Appendix A for the dose maps on a top view of the ANNI beamline). There was a substantial statistical improvement on measurements of the dose rates compared to the previous flux map (see Figure 16) calculated with the ESS proton source term. Even 70 cm thick layer of the heavy concrete was not efficient enough to obtain the 1.5 μSv/h requirement for the radiation safety as can be seen in Figure 23.

7.3 Simulations with the ANNI beamline Source Term Produced in This Project

As additional check that the test beamline source term is appropriate to be used for the ANNI beamline calculations, a simulation with the ANNI source term was carried out. The observed spectrum of neutrons at 22 m can be seen in Figure 24, and it is similar to the one calculated with the ESS test beamline source term (see Figure 18).

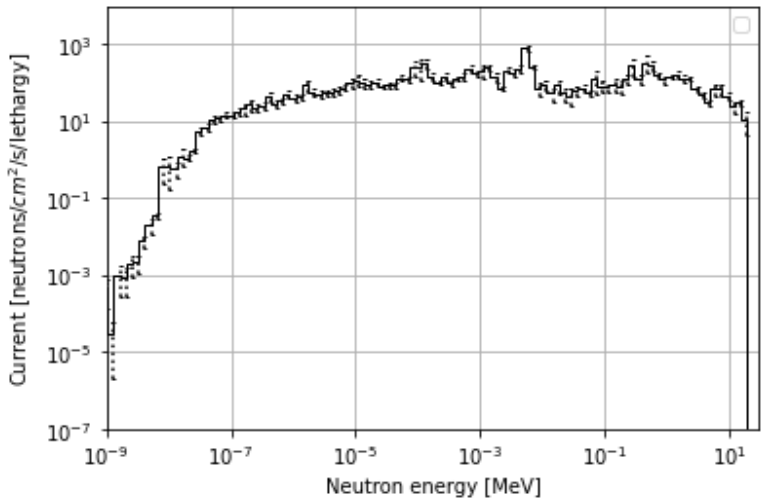

Figure 24: The spectrum of neutrons at x = 22 m measured in central part of the beamline axis. The ANNI beamline source term located at x = 2 m was used. Depicted based on the simulation with 70 millions of events.

8 Discussion

The spectrum at x = 22 m (see Figure 17) and neutron fluence (see Figure 16) through the beamline measured when the ESS proton source term was used clearly justified the use of the ESS test beamline, and ANNI beamline neutron source terms due to a large magnitude of the error and lack of readings outside the bunker (x > 15 m). The necessity to implement these source terms by means of a 2-step method is due to the difficulty of simulating the propagation of the neutrons over long distances.

It is noticeable on the spectrum measured at x = 22 m with all the source terms that the part containing the cold neutrons was heavily suppressed. This was observed due to the fact that the physics of neutron supermirrors (see Section 6.2) was not implemented in the simulations. Therefore, a large fraction of cold neu-

trons was lost, especially in the bent sections, as they did not reflect off the walls of the neutron guide but rather were captured by them. The reason behind neglecting the transportation of cold neutrons inside the neutron guides was due to the fact that the cold neutrons contribution is rather studied with different simulation codes, for example with Monte Carlo Simulation of triple axis spectrometers (McStas) [78] or Virtual Instrumentation Tool for the ESS (VITESS) [79]. Therefore, the transportation of cold neutrons through ANNI was not studied in this project. The experimental focus of this project was on simulations conducted with PHITS. More specifically, transportation of neutrons with energies >1 eV that represent a source of background was studied as a necessary step before conducting the neutron-sterile neutron oscillation experiments.

In addition, the spectra measured at x = 22 m revealed that there was a significant drop of fast neutrons as the neutrons propagated through the whole guiding system of the ANNI beamline. The reason for this flux reduction was the propagation of fast neutrons through the bent sections. However, there is also not enough statistics to draw conclusion about the residual contribution of fast neutrons with the highest energies above approximately 5×10^1 MeV.

The shapes of the spectra at x = 22 m produced by the ESS test beamline and ANNI beamline neutron source terms look similar. Therefore, it seems that the energy and angular distribution of neutrons passing through the opening of the test beamline could be generalised and used to define the spectrum of neutron source term for the ANNI beamline.

It is clear that the use of heavy concrete shielding with the thickness, even with the value of 70 cm, was not efficient enough to satisfy the ESS requirement. Namely, the effective dose outside the shielding could not exceed 1.5 μ Sv/h. It was expected that the thickness of the shielding that is constructed for a beamline with bent neutron guides did not exceed approximately 60 cm. Therefore, other solutions to provide efficient shielding should be studied. For example, by using shielding made of two layers. The first layer closest to the beam axis is then made of steel or similar high atomic number material which has the ability to slow down the fast neutrons. At the same time, the second layer is made of concrete or even high density concrete to stop the neutrons ultimately.

This project focused on the estimation of background produced by the fast neutrons. Nevertheless, there are other possible sources of background like cosmic background or background due to interaction of the cold neutron beam with the guide materials that require further studies beyond the scope of this project [1].

9 Conclusion and Outlook

In conclusion, the background consisting of fast neutrons was significantly reduced by the proposed ANNI beamline design. Consequently, a suppression of fast neutrons was observed in the spectrum at the position of 22 m from the center of the ESS target monolith. The ESS test beamline and ANNI beamline source terms provided more accurate results than the ESS proton source term. Moreover, the spectra produced by the ESS test beamline and ANNI beamline source terms were consistent and revealed that the the flux of fast neutrons peaked at about 10^2 neutrons/cm^2/s/lethargy.

The design of the guide system could be further optimised since a large fraction of fast neutrons were not stopped by the bunker wall but traveled below the neutron guide as can be seen in Figure 23. Moreover, additional studies that include the detector simulation for HIBEAM should be performed to estimate the impact of such residual background of neutrons to the sensitivity of the neutron in sterile neutron searches. These studies should also be expanded to include the beamstop for the regeneration mode and the neutron into antineutron oscillations.

The computation of radiation dose maps showed that a heavy concrete with the shielding thickness of 70 cm was not sufficient to satisfy the 1.5 μSv/h requirement from the ESS. The solution could be to use the two-layer shielding made of concrete and steel.

The studies performed in this project represent a first estimate of the background and radiation dose for the ANNI beamline. Thanks to these estimates, future optimization studies of the guide geometry will be performed. In addition, the results obtained in this project will be a part of the future proposal that will be submitted at the ESS for the construction of the ANNI beamline.

References

[1]A. Addazi, K. Anderson, S. Ansell, K. Babu, J. Barrow, D. Baxter, P. Bentley, Z. Berezhiani, R. Bevilacqua, C. Bohm, et al., "New high-sensitivity searches for neutrons converting into antineutrons and/or sterile neutrons at the european spallation source", arXiv preprint arXiv:2006.04907 (2020).

[2]B. Märkisch and T. Camille, *Report on particle and fundamental physics at ess*, tech. rep. (Technische Universität München, Mar. 2017).

[3]M. Baldo-Ceolin, P. Benetti, T. Bitter, F. Bobisut, E. Calligarich, R. Dolfini, D. Dubbers, P. El-Muzeini, M. Genoni, D. Gibin, et al., "A new experimental limit on neutron-antineutron oscillations", Zeitschrift für Physik C Particles and Fields **63**, 409–416 (1994).

[4]T. Sato, Y. Iwamoto, S. Hashimoto, T. Ogawa, T. Furuta, S.-i. Abe, T. Kai, P.-E. Tsai, N. Matsuda, H. Iwase, et al., "Features of particle and heavy ion transport code system (phits) version 3.02", Journal of Nuclear Science and Technology **55**, 684–690 (2018).

[5]S. Rigby, "Quarks are not behaving as they should, cern has found.", Science Focus (2021).

[6]G. Kane, *Modern elementary particle physics: explaining and extending the standard model* (Cambridge University Press, 2017), pp. 172–179.

[7]D. Lincoln, "What are hadrons, baryons and mesons?", Fermilab at work (2012).

[8]J. M. Cline, "Baryogenesis", arXiv preprint hep-ph/0609145 (2006).

[9]J. Wu, "Measurements of cosmic ray antiprotons with pamela and studies of propagation models", arXiv preprint arXiv:1205.5007 (2012).

[10]A. Aab, P. Abreu, M. Aglietta, I. Al Samarai, I. Albuquerque, I. Allekotte, A. Almela, J. A. Castillo, J. Alvarez-Muñiz, G. A. Anastasi, et al., "Observation of a large-scale anisotropy in the arrival directions of cosmic rays above $8\times$ 1018 ev", Science **357**, 1266–1270 (2017).

[11]O. Adriani, G. Barbarino, G. Bazilevskaya, R. Bellotti, M. Boezio, E. Bogomolov, L. Bonechi, M. Bongi, V. Bonvicini, S. Bottai, et al., "New measurement of the antiproton-to-proton flux ratio up to 100 gev in the cosmic radiation", Physical Review Letters **102**, 051101 (2009).

[12]M. Salamon, S. McKee, J. Musser, G. Tarle, A. Tomasch, C. Bower, R. Heinz, J. Miller, S. Mufson, S. Barwick, et al., "Limits on the antiproton/proton ratio in the cosmic radiation from 100 mev to 1580 mev", The Astrophysical Journal **349**, 78–90 (1990).

[13]C. J. Copi, D. N. Schramm, and M. S. Turner, "Big-bang nucleosynthesis and the baryon density of the universe", Science **267**, 192–199 (1995).

[14]B. Fields and S. Sarkar, "Big-bang nucleosynthesis (particle data group mini-review)", arXiv preprint astro-ph/0601514 (2006).

[15]W. Hu and S. Dodelson, "Cosmic microwave background anisotropies", Annual Review of Astronomy and Astrophysics **40**, 171–216 (2002).

[16]E. Gawiser and J. Silk, "The cosmic microwave background radiation", Physics Reports **333**, 245–267 (2000).

[17]L. Canetti, M. Drewes, and M. Shaposhnikov, "Matter and antimatter in the universe", New Journal of Physics **14**, 095012 (2012).

[18]V. Rubakov, "Cosmology", arXiv preprint arXiv:1504.03587 (2015).

[19]Z. Berezhiani and L. Bento, "Neutron–mirror-neutron oscillations: how fast might they be?", Physical review letters **96**, 081801 (2006).

[20]R. Aaij, C. A. Beteta, B. Adeva, M. Adinolfi, C. A. Aidala, Z. Ajaltouni, S. Akar, P. Albicocco, J. Albrecht, F. Alessio, et al., "Observation of c p violation in charm decays", Physical review letters **122**, 211803 (2019).

[21]D. E. Morrissey and M. J. Ramsey-Musolf, "Electroweak baryogenesis", New Journal of Physics **14**, 125003 (2012).

[22]R. Rangarajan, "Baryogenesis in the early universe", Pramana **53**, 1061–1067 (1999).

[23]A. Riotto and M. Trodden, "Recent progress in baryogenesis", Annual Review of Nuclear and Particle Science **49**, 35–75 (1999).

[24]D. E. Morrissey and M. J. Ramsey-Musolf, "Electroweak baryogenesis", New Journal of Physics **14**, 125003 (2012).

[25]A. M. Sirunyan, A. Tumasyan, W. Adam, F. Ambrogi, T. Bergauer, M. Dragicevic, J. Erö, A. E. Del Valle, M. Flechl, R. Fruehwirth, et al., "A measurement of the higgs boson mass in the diphoton decay channel", Physics Letters B **805**, 135425 (2020).

[26]P. Nath and P. F. Perez, "Proton stability in grand unified theories, in strings and in branes", Physics reports **441**, 191–317 (2007).

[27]F. P. Huang, P.-H. Gu, P.-F. Yin, Z.-H. Yu, and X. Zhang, "Testing the electroweak phase transition and electroweak baryogenesis at the lhc and a circular electron-positron collider", Physical Review D **93**, 103515 (2016).

[28]K. Babu, P. B. Dev, E. C. Fortes, and R. Mohapatra, "Post-sphaleron baryogenesis and an upper limit on the neutron-antineutron oscillation time", Physical Review D **87**, 115019 (2013).

[29]S. Patra and P. Pritimita, "Post-sphaleron baryogenesis and n n–$\overline{n}$ n' oscillation in non-susy so (10) gut with gauge coupling unification and proton decay.", The European Physical Journal C **74**, 1–13 (2014).

[30]K. Babu, R. Mohapatra, and S. Nasri, "Postsphaleron baryogenesis", Physical review letters **97**, 131301 (2006).

[31]Z. Berezhiani, "Through the looking-glass: alice's adventures in mirror world", in *From fields to strings: circumnavigating theoretical physics: ian kogan memorial collection (in 3 volumes)* (World Scientific, 2005), pp. 2147–2195.

[32]W. Tan, "Neutron oscillations for solving neutron lifetime and dark matter puzzles", Physics Letters B **797**, 134921 (2019).

[33]Z. Berezhiani, M. Frost, Y. Kamyshkov, B. Rybolt, and L. Varriano, "Neutron disappearance and regeneration from a mirror state", Physical Review D **96**, 035039 (2017).

[34]L. Randall, "What is dark matter?", Nature **557**, S6–S7 (2018).

[35]R. Foot, "Mirror dark matter: cosmology, galaxy structure and direct detection", International Journal of Modern Physics A **29**, 1430013 (2014).

[36]N. Malavasi, N. Aghanim, H. Tanimura, V. Bonjean, and M. Douspis, "Like a spider in its web: a study of the large-scale structure around the coma cluster", Astronomy & Astrophysics **634**, A30 (2020).

[37]L. Bento and Z. Berezhiani, "Leptogenesis via collisions: leaking lepton number to the hidden sector", Physical review letters **87**, 231304 (2001).

[38]Z. Berezhiani and A. Gazizov, "Neutron oscillations to parallel world: earlier end to the cosmic ray spectrum?", The European Physical Journal C **72**, 1–7 (2012).

[39]K. Greisen, "End to the cosmic-ray spectrum?", Physical Review Letters **16**, 748 (1966).

[40]J. Abraham, P. Abreu, M. Aglietta, E. Ahn, D. Allard, J. Allen, J. Alvarez-Muniz, M. Ambrosio, L. Anchordoqui, S. Andringa, et al., "Measurement of the energy spectrum of cosmic rays above 1018 ev using the pierre auger observatory", Physics Letters B **685**, 239–246 (2010).

[41]T. Abu-Zayyad, R. Aida, M. Allen, R. Anderson, R. Azuma, E. Barcikowski, J. Belz, D. Bergman, S. Blake, R. Cady, et al., "The cosmic-ray energy spectrum observed with the surface detector of the telescope array experiment", The Astrophysical Journal Letters **768**, L1 (2013).

[42]V. Santoro, K. Andersen, D. DiJulio, E. B. Klinkby, T. Miller, D. Milstead, G. Muhrer, M. Strobl, A. Takibayev, L. Zanini, et al., "Development of high intensity neutron source at the european spallation source", Journal of Neutron Research, 1–11 (2020).

[43]H. Danared, S. Kennedy, and M. Lindroos, "Ess under construction", CERN Courier (2020).

[44]K. Andersen, M. Guthrie, H. Wacklin-Knecht, A. Jackson, W. Schweika, P. Deen, A. Holmes, R. Toft-Petersen, A. Hiess, J. Taylor, O. Kirstein, S. P. Årsköld, S. Kennedy, and A. Schreyer, *The ess instrument suite – a capability gap analysis*, tech. rep. (European Spallation Source, Oct. 2018).

[45]G. J. Russell, *Spallation physics*, tech. rep. (1991).

[46]R. Garoby, A. Vergara, H. Danared, I. Alonso, E. Bargallo, B. Cheymol, C. Darve, M. Eshraqi, H. Hassanzadegan, A. Jansson, et al., "The european spallation source design", Physica Scripta **93**, 014001 (2017).

[47]T. Soldner, H. Abele, G. Konrad, B. Märkisch, F. M. Piegsa, U. Schmidt, C. Theroine, and P. T. Sánchez, "Anni–a pulsed cold neutron beam facility for particle physics at the ess", in Epj web of conferences, Vol. 219 (EDP Sciences, 2019), p. 10003.

[48]Z. Berezhiani, "More about neutron–mirror neutron oscillation", The European Physical Journal C **64**, 421–431 (2009).

[49]C. Vigo, L. Gerchow, B. Radics, M. Raaijmakers, A. Rubbia, and P. Crivelli, "New bounds from positronium decays on massless mirror dark photons", Physical review letters **124**, 101803 (2020).

[50]A. Y. Ignatiev and R. Volkas, "Geophysical constraints on mirror matter within the earth", Physical Review D **62**, 023508 (2000).

[51]G. Ban, K. Bodek, M. Daum, R. Henneck, S. Heule, M. Kasprzak, N. Khomutov, K. Kirch, S. Kistryn, A. Knecht, et al., "Direct experimental limit on neutron–mirror-neutron oscillations", Physical review letters **99**, 161603 (2007).

[52]A. Serebrov, E. Aleksandrov, N. Dovator, S. Dmitriev, A. Fomin, P. Geltenbort, A. Kharitonov, I. Krasnoschekova, M. Lasakov, A. Murashkin, et al., "Experimental search for neutron–mirror neutron oscillations using storage of ultracold neutrons", Physics Letters B **663**, 181–185 (2008).

[53]I. Altarev, C. Baker, G. Ban, K. Bodek, M. Daum, P. Fierlinger, P. Geltenbort, K. Green, M. van Der Grinten, E. Gutsmiedl, et al., "Neutron to mirror-neutron oscillations in the presence of mirror magnetic fields", Physical Review D **80**, 032003 (2009).

[54]K. Bodek, M. Kuźniak, J. Zejma, M. Burghoff, S. Knappe-Grüneberg, T. Sander-Thoemmes, A. Schnabel, L. Trahms, G. Ban, T. Lefort, et al., "Additional results from the first dedicated search for neutron–mirror neutron oscillations", Nuclear Instruments and Methods in Physics Research Section A: Accelerators, Spectrometers, Detectors and Associated Equipment **611**, 141–143 (2009).

[55]A. Serebrov, E. Aleksandrov, N. Dovator, S. Dmitriev, A. Fomin, P. Geltenbort, A. Kharitonov, I. Krasnoschekova, M. Lasakov, A. Murashkin, et al., "Search for neutron–mirror neutron oscillations in a laboratory experiment with ultracold neutrons", Nuclear Instruments and Methods in Physics Research Section A: Accelerators, Spectrometers, Detectors and Associated Equipment **611**, 137–140 (2009).

[56]Z. Berezhiani and F. Nesti, "Magnetic anomaly in ucn trapping: signal for neutron oscillations to parallel world?", The European Physical Journal C **72**, 1–7 (2012).

[57]Z. Berezhiani, R. Biondi, P. Geltenbort, I. Krasnoshchekova, V. Varlamov, A. Vassiljev, and O. Zherebtsov, "New experimental limits on neutron–mirror neutron oscillations in the presence of mirror magnetic field", The European Physical Journal C **78**, 1–12 (2018).

[58]C. Abel, N. J. Ayres, G. Ban, G. Bison, K. Bodek, V. Bondar, E. Chanel, P.-J. Chiu, C. Crawford, M. Daum, et al., "A search for neutron to mirror-neutron oscillations using the nedm apparatus at psi", Physics Letters B **812**, 135993 (2021).

[59]Y. N. Pokotilovski, "On the experimental search for neutron→ mirror neutron oscillations", Physics Letters B **639**, 214–217 (2006).

[60]Z. Berezhiani, M. Frost, Y. Kamyshkov, B. Rybolt, and L. Varriano, "Neutron disappearance and regeneration from a mirror state", Physical Review D **96**, 035039 (2017).

[61]E. S. Golubeva, J. L. Barrow, and C. G. Ladd, "Model of n annihilation in experimental searches for n transformations", Physical Review D **99**, 035002 (2019).

[62]J. L. Barrow, E. S. Golubeva, E. Paryev, and J.-M. Richard, "Progress and simulations for intranuclear neutron-antineutron transformations in $^{40}_{18}$Ar", Physical Review D **101**, 036008 (2020).

[63]N. Cherkashyna, R. J. Hall-Wilton, D. D. DiJulio, A. Khaplanov, D. Pfeiffer, J. Scherzinger, C. P. Cooper-Jensen, K. G. Fissum, S. Ansell, E. B. Iverson, et al., "Overcoming high energy backgrounds at pulsed spallation sources", arXiv preprint arXiv:1501.02364 (2015).

[64]V. Santoro, X. X. Cai, D. DiJulio, S. Ansell, and P. M. Bentley, "In-beam background suppression shield", Journal of Neutron Research **18**, 135–144 (2015).

[65]G. Scionti, R. Agostino, D. Colognesi, G. Gorini, M. Hartl, V. Santoro, and R. Senesi, "Neutronic calculations for the shielding design of the vespa instrument at the european spallation source", Journal of Surface Investigation: X-ray, Synchrotron and Neutron Techniques **14**, S190–S194 (2020).

[66] *The swedish radiation safety authority*, www.stralsakerhetsmyndigheten.se/en, Accessed: 2021-03-10.

[67] G. Muhrer and K. Sigrid, *Ess procedure for designing shielding for safety.* Tech. rep., Internal ESS document (European Spallation Source, 2019).

[68] G. Muhrer and F. Javier, *Definition of supervised and controlled radiation areas*, tech. rep., Internal ESS document (European Spallation Source).

[69] R. F. Barth, A. H. Soloway, and R. G. Fairchild, "Boron neutron capture therapy for cancer", Scientific American **263**, 100–107 (1990).

[70] S. Hashimoto, *Phits ver. 3.20 user's manual*, tech. rep. (Japan Atomic Energy Agency, Apr. 2020).

[71] E. Gabriel and G. E. Fagg, "Open mpi: goals, concept, and design of a next generation mpi implementation", in European parallel virtual machine/message passing interface users' group meeting (Springer, 2004), pp. 97–104.

[72] V. Santoro, D. DiJulio, S. Ansell, N. Cherkashyna, G. Muhrer, and P. M. Bentley, "Study of neutron shielding collimators for curved beamlines at the european spallation source", in Journal of physics: conference series, Vol. 1046, 1 (IOP Publishing, 2018), p. 012010.

[73] E. S. Source, *Comblayer*, http://plone.esss.lu.se/, Accessed: 2021-03-12.

[74] D. Drosdoff and A. Widom, "Snell's law from an elementary particle viewpoint", American journal of physics **73**, 973–975 (2005).

[75] R. Gähler, *Neutron optics and polarization.* NIST Center for Neutron Research. www.ncnr.nist.gov/summerschool/ss09/pdf/Chupp_FP09.pdf, Accessed: 2021-04-11.

[76] W. Schweika, *Ess instrument construction proposal dream (powhow)*, tech. rep. (European Spallation Source, Mar. 2014).

[77] V. Santoro, D. D. Julio, P. Bentley, and L. Zanini, *Source term for shielding design of bunker and beamlines at ess.* Tech. rep. (European Spallation Source, Oct. 2018).

[78] K. Lefmann and K. Nielsen, "Mcstas, a general software package for neutron ray-tracing simulations", Neutron news **10**, 20–23 (1999).

[79] G. Zsigmond, K. Lieutenant, and F. Mezei, "Monte carlo simulations of neutron scattering instruments by vitess: virtual instrumentation tool for ess", Neutron News **13**, 11–14 (2002).

A The dose maps on a top view of ANNI depicted to test the effectiveness of the shielding

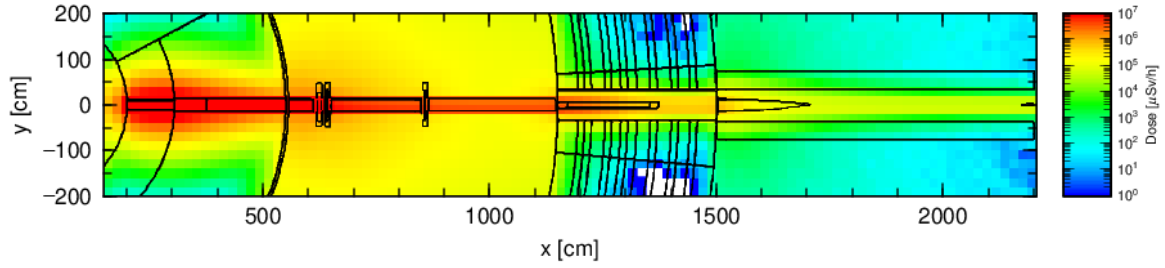

(a)

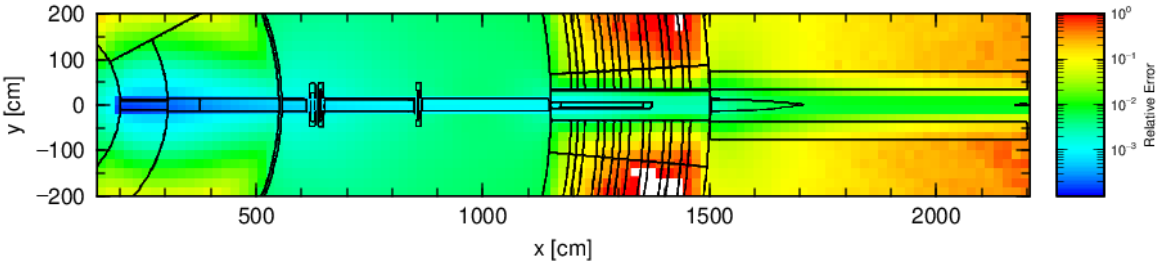

(b)

Figure 25: The dose map of neutrons for 40 cm thick concrete shielding of ANNI is shown on Figure 25a. Relative error for the dose map is shown in Figure 25b. The shielding was tested outside the bunker wall between 15 and 22 m. Depicted based on the simulation with 1500 million of events. The test beamline source term defined at 2 m was used. The view on ANNI is from the top.

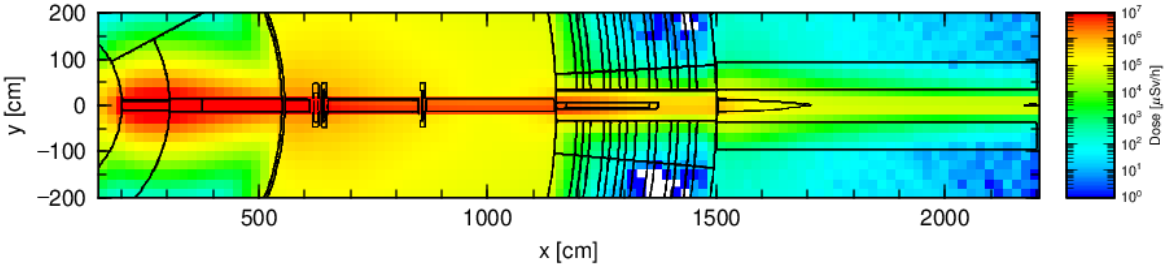

(a)

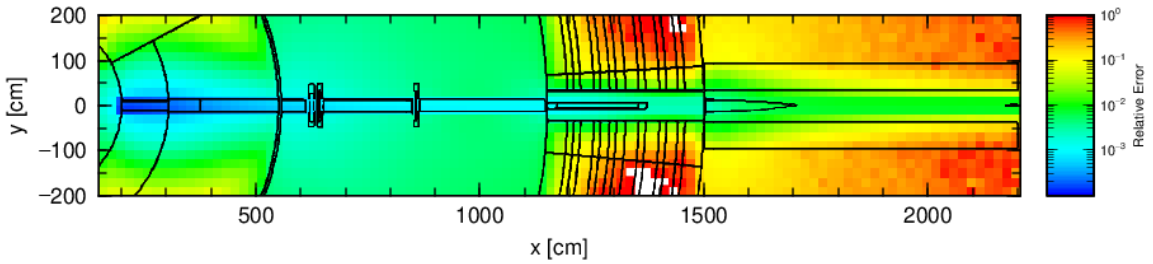

(b)

Figure 26: The dose map of neutrons for 60 cm thick concrete shielding of ANNI is shown in Figure 26a. Relative error for the dose map is shown in Figure 26b. The shielding was tested outside the bunker wall between 15 and 22 m. Depicted based on the simulation with 1500 million of events. The test beamline source term defined at 2 m was used. The view on ANNI is from the top.

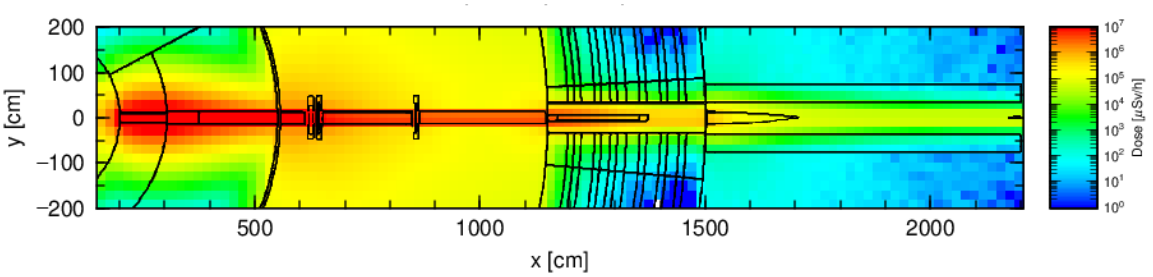

(a)

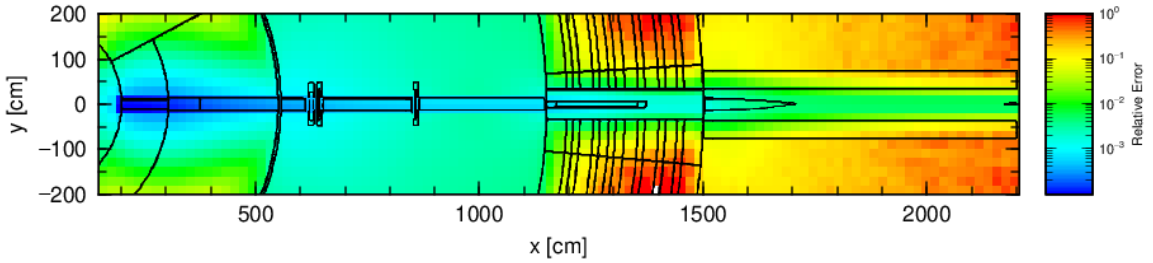

(b)

Figure 27: The dose map of neutrons for 40 cm thick high density concrete shielding of ANNI is shown in Figure 27a. Relative error for the dose map is shown in Figure 27b. The shielding was tested outside the bunker wall between 15 and 22 m. Depicted based on the simulation with 1500 million of events. The test beamline source term defined at 2 m was used. The view on ANNI is from the top.

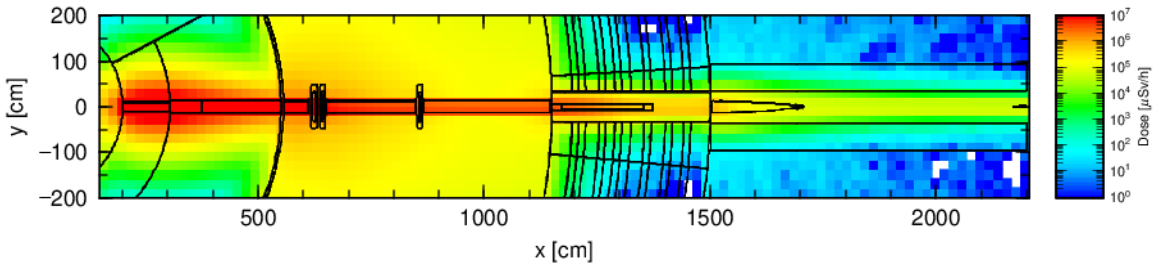

(a)

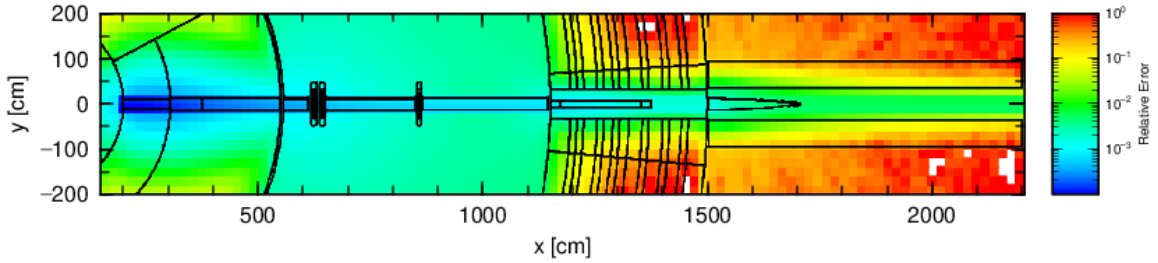

(b)

Figure 28: The dose map of neutrons for 60 cm thick high density concrete shielding of ANNI is shown in Figure 28a. Relative error for the dose map is shown in Figure 28b. The shielding was tested outside the bunker wall between 15 and 22 m. Depicted based on the simulation with 1500 million of events. The test beamline source term defined at 2 m was used. The view on ANNI is from the top.